

# Response to Reviewers, ACP-2019-34

David Ian Duncan, Patrick Eriksson, Simon Pfreundschuh, Christian Klepp, and Daniel C. Jones

## General response

Thanks to both reviewers for the in depth and thoughtful comments offered on ways to improve this manuscript. In accordance with suggestions from both reviewers, the follow major additions have been made: a figure showing OceanRAIN sampling (Fig. 1), a table with OceanRAIN size bins (Table 1), a figure with OceanRAIN and GPM  $N_w$  vs.  $D_m$  (Fig. 3), more panels to  
5 elucidate the PDF differences in the normalized gamma space (now Fig. 11), and a penultimate section to separate better the results from discussion. The title has also been modified. The histograms of GPM and OceanRAIN data separated by latitude are also now presented in a different plot format due to reviewer and public comments, and all GPM data used for analysis have been updated from V05 to V06 to make the analysis as up to date as possible. The reviewers' comments have led to refinement of the manuscript's language in numerous places throughout the paper.

10 In the following, the reviewers' comments are given in italics, with specific responses following each and any additional text added to the manuscript then given in quotes. Changes to the manuscript are also visible in the 'tracked changes' document uploaded alongside this response.

## Reviewer 1

*Specific to the last sentence in the Abstract: Please see Munchak, et al., 2012: "Relationships between the Raindrop Size  
15 Distribution and Properties of the Environment and Clouds Inferred from TRMM", J. Climate, 25, 2963–2978. This is a relevant paper.*

This sentence has been removed from the abstract, as it was not presented in clear language.

*General: Note that MGD is sometimes refers to G-G, see for example, Petty, G. W., and Huang, W. The modified gamma size distribution applied to inhomogeneous and non-spherical particles: Key relationships and conversions. J. Atmos. Sci. 2011:  
20 Vol. 68, pp. 1460–1473.*

This is now stated explicitly in the second paragraph of the introduction to be clear on this point.

*Page 2, line 5: Refer to Testud et al here.*

Done

*Page 3, line 31: What is the size resolution of the ODM?*

25 The size bins used by the ODM are now contained in the text as Table 1. Because there are 120 size bins in the dataset and not all of these are relevant for readers, 60 are given in the table.

Page 4, line 4: Please clarify "impacts of turbulence"

To clarify this, the following has been added to S2.1: "A wind vane turns the disdrometer to keep the optical path normal to the wind direction, and the disdrometer's cylindrical volume ensures that the incident angle of hydrometeors does not affect the measurement. These work in concert to minimize impacts of turbulence from local up- and down-drafts, to limit under-  
5 catchment and drops impacting the sensor from various directions (Klepp, 2015)."

Page 4, para 3: It's not clear why the accuracy should depend on oceanic or continental cases. Bumke and Seltman showed that the average DSD shapes were similar in coastal and continental locations. They used the scaling of Sempere-Torres et al to fit the coastal and continental DSDs and found an invariant shape. Perhaps this should also be mentioned here.

This paragraph was originally added on the suggestion of the editor, to give a sense of the trustworthiness of the derived DSD  
10 parameters and whether the accuracy of the derived parameters varies for different regimes. To clarify, we are not suggesting that the accuracy of derived DSD parameters would depend on the location, but rather there may be regime-dependent biases owing to the sensitivity of the instrument that would have an impact on the derived parameters. In the text we have added the following sentence to make this clearer: "In other words, the accuracy DSD parameters reported by OceanRAIN may exhibit bias in regimes with many small drops below the disdrometer's sensitivity threshold or for distributions with a shape unlike  
15 that assumed."

Page 7, end: Recommend plotting  $N_w$  vs  $D_m$  on semi-log scale to further illustrate the inverse correlation between the two, for ODM and GPM.

This is now included in the manuscript as the new Fig. 4.

Page 9, line 5: It's not clear why  $\mu=2$  fits the mode of the normalized DSD shape in fig. 3 especially for  $D/D_m < 0.5$ . In fact  
20  $\mu=-2$  appears to be better.

Interpretation of this figure was a little tricky due to the color scale being saturated and the very high density of points in the middle of the figure. To show this better, the figure's color scale has been modified to hopefully be clearer and more differentiable for readers.

Page 9, line 15: Please clarify this range for  $\mu$  for tropical cases. The  $\mu$  estimate is very sensitive to the shape of the small  
25 drop end. It is not clear what the resolution and accuracy are for the ODM at tiny-small sizes. No independent evaluation of the ODM accuracy is given for the small drop end. Hence, caveats are recommended when statements regarding  $\mu$  ranges are given.

This has been modified to be less declarative: "...ranging roughly between  $\mu = 0$  to  $\mu = 3$ ..." and the point regarding ODM's insensitivity to small drops is well taken. Caveats regarding this insensitivity are now present in various places within the  
30 revised manuscript.

Page 10, line 2: What is meant by "moments" in this context? Are you referring to the moment-based estimation of  $\mu$ ?

This was unclear and inconsistent in the manuscript, sometimes tending towards the usage in modeling such as single or double moment microphysics. To make this clearer, different versions of the MGD are now specifically defined in Section 2.1 and referred to in terms of 'parameters' used instead of 'moments.'

35 Page 11, line 6: use of "power" is not conventional...please use another descriptor.

This sentence has been modified: "...the MGD with a low  $\mu$  value lies near the highest probability densities of the observed PDF."

*Page 11, line 15: the moments fit should be explained earlier.*

This terminology has been modified and is now stated earlier in the manuscript, in Section 2.1.

- 5 *Page 11, line 15: Units for RWC are not clear....seems like mg/m<sup>3</sup>. No discussion of fig.5 ? Except for second panel, the remaining GMM are not close to the measured N(D).*

The units of the RWC for the figure are now reiterated in the caption to be clearer. Discussion of the original Fig. 5 is now included as a new paragraph, as this was indeed lacking before.

- 10 *Page 12, line 2: At this point, recommend that the 4-parameter gamma be used to illustrate that 2 shape parameters are needed.*

The following sentence was added to that paragraph: "It is an indication that a second shape parameter may be useful for describing oceanic DSDs, in line with the generalized gamma approach argued for by Thurai and Bringi (2018)."

- 15 *Page 17, line 5: The conclusion is based on the assumption that the resolution and accuracy of N(D) from ODM for small drops is well-established but this has not been demonstrated. The use of total accumulation is not the only criteria by which one justifies the use of the MGD. The width of the mass spectrum is considerably increased when the small drop end is accurate. From cloud physics viewpoint the N(D) is a result of various microphysical processes that are controlled by the low order moments including M0. The GPM algorithms use path integrated attenuation as a constraint...the attenuation is also sensitive to the small drop end especially at Ka-band.*

- 20 This is a good point regarding GPM's use of PIA, and this has been added to the description of the measurement vector used by GPM CORRA in Section 2.2.

*Page 17, line 29: What about stratiform vs convective vs shallow rain types?*

This was addressed somewhat in the first paragraph of S3.1, in that from a retrieval perspective, a priori categorization of precipitation into stratiform/convective/other types is highly dependent on ancillary information or just not feasible.

## **Reviewer 2**

- 25 *1. Reorganize to separate Data Information / Tools (the datasets, their intricacies, and the models you ran them through) from Results (what your methods produced) from Discussion (as a logical conclusion of the results shown, what do the results mean?; what are the implication of results based on the methods you used?). Right now, methods, results, and discussion are mixed throughout each paragraph. This often means the authors often repeat themselves. ... The most egregious instances of mixing discussion with results are in Sec. 3. ...*

- 30 In response to this comment, the paper has been restructured to separate results explicitly from discussion. A separate discussion section now exists before the summary and conclusions.

*2. Rewrite/Revise each sentence for literal truth. Each statement should be made to be physically true, word for word. So many of the sentences in this paper contain vague, non-specific, perhaps physically impossible language that is abstract*

and doesn't really teach the reader anything. The authors need to more specific detail in several places so that their results are digestible, understandable, and reproducible. In many cases, I did not understand what the authors even did in terms of methods, how they drew the conclusions stated, what certain plots really showed, or how to draw conclusions from these plots. In many cases, problems/issues are alluded to (e.g. uncertainty, constraints, sensitivity), but the specifics or causes of these  
5 problems are withheld so the reader is left with suspense - what could the problems really be and why are they there? We don't know, because the authors allude to issues without explaining them.

Responses to the reviewer's specific examples, ranging from a-u, follow here: (a) 'easily' has been removed, but the remainder of the sentence stands, as it is a general statement about a statistical method so it does not to be justified in specific physical terms at this stage. (b) It is permissible to use 'underpin' to mean 'support' and the ODM does support the OceanRAIN data  
10 collection. (c) The sensitivity of DPR is now given in dBZ in Section 2.2, but the exact sensitivity in terms of drop sizes is not addressed as this is not straightforward. It depends on both size and concentration, and most GPM literature rather quotes minimum detectable rain rates, which is less applicable here for a discussion on DSD. (d) 'more' has been removed. (e) Many instances of 'common' have been replaced with other words. (f) Discontinuity here simply meant bins with zero counts in  
15 between bins with positive counts, visualized in Fig. 7. There is no systematic instrument error reported, but we assume that some random error does exist. (g) Removed. (h) The authors feel this is justified despite being metaphorical, because it conveys the sentiment accurately that GMM does not solve the DSD representation issue in one fell swoop. (i) Done. (j) Changed to 'clearly different.' (k) 'Functional form' is used in the manuscript to mean the mathematical construct such as MGD, whereas 'model' and 'fit' are used in different contexts in the manuscript. (l) 'Under/Un-constrained' in retrieval terms means that there is less information than unknowns, now stated explicitly in the text: "...an under-constrained problem (more unknowns than  
20 information)..." (m) Changed to "conserve total RWC" (n) Removed 'particularly.' (o) 'This' was changed to "The calculated rain rate" to clarify this sentence. (p) Modified to "higher number concentrations occur over warmer ocean surfaces..." (q) This statement is purposefully vague as it is about various differences, pointed to by the two citations offered and elucidated by the subsequent sentences. (r) All instances of 'bulk' have been removed or modified. (s) Many of these words have been removed or modified in the manuscript. Regarding under- vs. over-representation, it should be clear from the text and figure that it refers  
25 to whether the frequency of occurrence is lower or higher than that observed. (t) Posterior is a standard phrase in optimal estimation methodology and needs to be retained. (u) This has been clarified to "not always well represented by the 3-parameter MGD."

3. I'm unsure about the title after reading the paper. The authors conclude that there are several forms of DSD shape/solution, all of which overlap a bit, and their large datasets include instances of DSD that oscillate around these forms (as shown by  
30 the machine learning). Then they make conclusions about how well in situ observations of DSDs are represented with current satellite DSD retrievals (sensitivity problems appear to limit the capabilities of the satellites), and how much scatter should exist in satellite retrieved  $Z_h$  and  $T_b$  given the observed DSD (quite a bit, and it varies based on frequency). The paper really doesn't separate out "raindrop regimes"... which would indicate to me to be physical distinctions like monsoon phases, convective v. stratiform, different meteorological conditions, etc. Perhaps the impact and message of the paper is best summarized as: "On  
35 the distinctiveness of oceanic raindrop distributions in observations and satellite measurements"

The word 'regime' is indeed quite loaded in this context, and not used specifically enough to be justified. With this in mind, the authors have decided to change the title to "On the distinctiveness of observed oceanic raindrop distributions" and removed the use of 'regime' in that context elsewhere in the manuscript.

4. *In intro: "A lack of globally representative DSD"... do we lack that? What is lacking, specifically? Are you saying that we need to find a single DSD that represents all DSD across the globe (implied by the way this is written), or that we need a representative dataset? Unclear.* 5. *The authors don't give enough credit to the oceanic-ish DSD measurements that are still being reported at Manus Island and Kwajalein Atoll. These are not representative of other DSD in other regions, but they do contribute something important; not all the DSD studies have been confined to land or coast (Thompson et al. 2015 and 2018, and this data is also used in Dolan et al. 2018).*

10 The language here was not clear, and it now reads as simply "global DSD data." In addition, because the issue of a globally representative DSD data set is important to the paper's justification, the following has been added to the end of the paragraph: "It is thus desirable to have measurements of DSDs over ocean, and crucial that these measurements are globally representative rather than skewed toward one region or another." On the second point here the reviewer is quite right, and we now acknowledge the importance of data from these sources: "...observations of DSDs over ocean have mostly been limited to field campaigns, a few small tropical islands and atolls, and coastal radar retrievals."

6. *The authors make up a quantity of RWC and RWP, when it seems that literature to-date uses LWC and LWP to mean the same thing. Paper should conform to these precedents instead of inventing or using their own terminology. It's clear in the paper that only rain cases are used, not ice- or mixed-phase precip, at least at the ground.*

20 The terminology used is perhaps not standard everywhere, but is quite common for discussing precipitation in retrievals and models, especially when it is desirable to differentiate between hydrometeor types. Indeed the GPM algorithms differentiate between cloud LWP, RWP, GWP, IWP, as these all behave quite differently with regard to the radiative transfer. Our reasoning for this is now given before RWP is defined: "Here we differentiate between cloud water and rainwater due to their different radiative characteristics, with the total liquid water path being the sum of the two."

7. *Fig. 2 - each of the plots must be spaced farther apart in the Latitude dimension so that the distributions can be viewed as distinct. The plots run into each other and cannot be distinguished one from the other. Therefore, the point of this plot is lost. Also, It's not clear what the latitude averaging bin width was here. It's centered 20deg apart - is that the center value +/- 10 deg in each direction? Explain in text and caption*

This figure has been changed to a different style of plot that should make interpretation much simpler for readers.

8. *The units of Nw need to be checked - it's often discussed in the text as Nw when it's really logNw that is plotted. The parentheses should be adjusted to explain the units properly. log10(Nw [mm-1 mm-3]). Log10Nw doesn't have the same units as Nw itself.*

This has been rectified in the figure caption and the figure itself.

9. *Each of the box and whisker plots need a legend that explain the box width, lines dots, cross hairs (what are the percentiles, etc.). It's too much work to read the caption and try to interpret the plot at the same time.*

35 These are now more explicitly stated in the figure caption.

10. Add a plot of the map of observations used, so that your Fig. 1 and comparisons between latitude bands can be better understood. The text mentions that more or less data was collected in certain regions, but the reader can't deduce that because no plot of the data extent is shown.

Done.

5 11. Fig. 4 is just about incomprehensible. The conclusions about this figure do not appear to stem logically from the plot, and the plot itself is confusing. If you are making a comparison between models and obs, that is one thing and can be shown a certain way. Then if you also want to compare latitude bands, you should show the PDFs from those latitude bands first before you plot the difference. The difference here doesn't really make sense either because it doesn't seem physical to subtract a tropical PDF from a higher lat PDF; the result doesn't really have any physical significance (or at least the significance is  
10 not well-explained or logical). Suggest deleting Fig. 4 and showing the real tropical and high latitude PDFs. Then see if your stated conclusions are supported by the real data. The entire discussion of Fig. 3-4 needs to be carefully curated to be sure that the interpretations of the authors are readily apparent from the plots shown; I couldn't really see how they made all the conclusions that were stated. Particularly the regional dependence, but also the under vs. over "representation" issue. Fig. 4 needs titles to distinguish them and explain more about what is shown.

15 This figure has been completely redone to be clearer.

12. I kept forgetting what GMM and MGD meant. . . these acronyms are used throughout and their physical significance became lost several pages in. Suggest using plain language. See Fig. 5 - it's not clear what the significance of the acronyms are for the purposes of showing the data.

While the authors admit that there are many acronyms used in the text, especially around that figure, neither GMM nor MGD  
20 can easily be replaced by 'plain language' without something being lost or the text becoming much more wordy. For example, MGD needs to be differentiated from generalized gamma (which is also discussed) and the Petty and Huang (2011) paper we cite uses this acronym. GMM is the standard way to refer to Gaussian Mixture Models in the literature as well, and using plain language such as 'the machine learning technique' would be less specific and more wordy.

13. Typesetting should be improved a. The lack of line numbers on each line makes it difficult for the reviewer to suggest  
25 particular comments and corrections in each case. The authors should number each line in the future. b. The paragraphs would also be easier to distinguish if their indentation was larger. It kind of all runs together c. The references within parentheses are wrong. For example this is typed often: (also used by Duncan et al. (2019)) < see double parentheses at end here. d. Most journals forbid sentences to begin with the name of the variable and will insert words to rectify this situation, whether or not it makes physical sense. The authors are encouraged to fix this the way they want before it gets changed for them (see paragraph  
30 above equations on page 2). Completing these sentences also will help ground them in concrete, physical terms: e.g. correcting to be: "The values of  $N_0$  and  $NW$ . . ."

The reviewer's first two typesetting suggestions are counter to the style of ACP and the EGU journals. The manuscript was prepared with the ACPD Latex template, and thus the typesetting should be in accordance with ACPD articles. The latter two points, c and d, have been amended in the text wherever found.

35 14. Equation (3) is really 3 equations. . . separate them?

Done

15. *N<sub>w</sub>* is normalized by LWC. make this clear in its discussion on page 2 and elsewhere.

Done

16. Petkovic et al. 2018 reference page 2 - this is not the definitive nor the first paper to study these things. Reference prior  
5 work more appropriately to justify this statement - other canonical papers?

The recent study cited is indeed not canonical and is more relevant for ice hydrometeors anyway. It has thus been removed.

17. References are made to OceanRAIN-M . . . what is the -M??? Not defined.

At its first introduction, OceanRAIN-M is now defined: "Specifically, the OceanRAIN-M ("OceanRAIN Microphysics")  
data..."

10 18. The ODM470 doesn't sense drops smaller than 0.4 mm because the voltages are too noisy below this inferred level  
(the sensitivity is incorrectly stated as 0.3 in the manuscript). From Klepp 2018: "The first 12 bins ranging from 0.04 to  
0.36mm in size are not recorded because they are prone to contain artificial signals caused by ship vibration." This is a  
significant downside to the instrument that needs to be explicitly stated in the manuscript. A large portion of the DSD spectrum  
is contained below this level (Thompson et al. 2015, Thurai et al. 2018). Also, the ODM assumes a fall velocity and does a  
15 vector mean of the fall velocity + wind through sensor. This is an approximation and, in my interpretation of the ODM methods,  
a potential source of error in the computed number density. 19. "Is an issue faced by all disdrometers" -> yes, but it's the worst  
for ODM compared to other disdrometers currently used. See comment above.

The following has been added to address this, as it is indeed worth stressing: "To be clear, there can be significant number  
concentrations below this sensitivity limit, but voltages corresponding to drops less than 0.36 mm are disregarded as these can  
20 be contaminated by vibrations from the ship (Klepp et al., 2018) and this is a key drawback of the data set."

20. Minimize effects of turbulence -> minimize under-catchment of drops and minimize the effect of drop splashing against  
the sensor from multiple directions. Turbulence will still exist. It's just that the orientation of the instrument attempts to catch  
as many drops as it can.

This is duly noted and has been corrected. See response to Reviewer 1 above.

25 21. Why would the disdrometer NOT "show no difference in accuracy between oceanic and continental cases"? Why would  
differences occur? It should work the same, except that while at sea, it has to reorient into the wind and a vector mean  
calculation is done to assume fall velocity+wind through the sensor, which could be susceptible to flow distortion.

This was also addressed in response to Reviewer 1 above.

22. Introduction of the "Combined Data" is confusing. The heading of that subsection is also confusing. What does it mean?

30 The authors admit that it is confusing, but the GPM project is not consistent when referring to this data set, even internally.  
The definitive paper by Grecu et al. (2016) is titled "The GPM Combined Algorithm" but never introduces any acronym,  
whereas some other GPM publications use the acronym CORRA. It is perhaps less confusing if CORRA is introduced as an  
acronym and used throughout, so that is what we have elected to do. The subsection title has been changed in accordance.

23. State the different vertical resolutions of the two DPR frequencies. It's mentioned that they differ, but not what they  
35 actually are.

The vertical resolutions do not differ in normal scanning (NS) mode. From Hou et al. (2014): "Both radars have a nominal vertical range resolution of 250 m, sampled every 125 m, with a minimum detectable signal of better than 18 dBZ." In high sensitivity (HS) mode these differ, but we are not using HS data in this study.

24. *The specifications of the GMI and DPR (geometry, resolution) are scattered about the last paragraph of 2.2. Make it more concise.*

These are only scattered this way because they are germane to interpretation of CORRA, whereas earlier description of GPM was about the satellite itself. Readers can consult the cited literature if they desire those details.

25. *"Ground-based data from Ocean-RAIN-M" — Ocean rain is over ocean! Not land.*

All references to "ground-based" have been changed to "surface-based."

26. *How is clutter classified in satellite retrievals? Sec. 2.2. Seems like it would impact your analysis.*

For the methods of dealing with surface clutter, we will defer to the JAXA documentation on radar processing for DPR. It is not especially important for the discussion here as it is less of a concern over ocean, and DPR's relatively fine 250m vertical resolution means that the data will not witness big vertical jumps from one pixel to another. As we are just using histogram data from the level 3 monthly product and not pixel (level 2) data here, it is deemed of lesser importance for discussion.

27. *Provide citation for GMM upfront at its first introduction*

Done

28. *90,000 points seems REALLY low compared to the size and length of time of the OceanRAIN dataset. Is this correct? I've collected ODM data over a month and gotten more than 40,000 points of usable data.*

This is correct. From Klepp (2018), 3-4% of the total 6.83 million minutes of observations in OceanRAIN contain rain rates above  $0.1 \text{ mm h}^{-1}$ . In addition, the screening process we use requires that each point be 'rain definite' by the flag provided, contain at least 50 drops measured, and have the MGD fit parameters given. These last two criteria ensure there will be a proper distribution of drops, as OceanRAIN only provides  $D_m, N_w, \mu$  if "the PSD has at least 10 size bins filled with data" (Klepp 2018). Thus the total number of cases is only a fraction of the total 'raining minutes' measured by OceanRAIN. To make this clearer, the text has been amended thus: "Only data points marked as rain definite, with 50 or more measured drops, and with a probability of precipitation of 100% were used in the following analysis. To be consistent, only data points with measurements in ten or more size bins are used (Klepp et al., 2018), as these provide the parameters from the MGD fit to Eq. 3."

29. *What are the size ranges of the 60 size bins? And what are their approximate spacing?*

As in response to Reviewer 1 above, a table of the bin sizes is now included as Table 1.

30. *In several places, the authors assert that assumptions and fits haven't been used on DSD obs, but then they say that the data are normalized and that a "nominal shape parameter is assumed" ... This seems contradictory. And the authors fail to mention how the data are normalized - by liquid water content? Similar to  $N_w$ ? how was the parameter chose?*

Perhaps this is confusing, but it is not contradictory as we are discussing the data used in different contexts. This is now addressed with a separate paragraph in Section 2.1 and clarified in the results section as well when presented.

31. *Provide citation of BIC when introduced*

Done

32. *The authors make claims that they are testing for differences in DSD in different regions or locations, but really they only separated data into very wide latitude bands (Fig. 1, Fig. 2). This distinction, and the implication of the real results, need to be me explicit so as not to overstate the significance or conclusions. Search all uses of “region” and “location” to determine whether you actually mean “latitude”* 33. *Similarly, the authors make mention of a stratocumulus region, but have not proven where this is or justified their interpretation of that based on a map of the data - which should be added to justify statements made throughout the analysis in Sec. 3*

This is a good point, and all unspecific instances of using 'region' or 'location' have been amended. However, some of the discussion of the distinctiveness of GMM shapes did look into regional occurrences and thus this discussion has been maintained despite not being shown explicitly in this manuscript.

10 34. *The differences in DSD based on SST seem readily explainable from the Clausius Clapeyron equation - warmer SST leads to higher saturation vapor pressure of air, so moisture content can be higher. – see Fig. 1 and Fig. 2. Nw is directly proportional to LWC (your eq. 3), so result of Fig. 1 lower right is awesome but perhaps not surprising.*

Indeed, and the text has been amended to include mention of C-C: "..., as may be expected due to the Clausius-Clapeyron equation."

15 35. *“Blue” dots in Fig. 2 don’t show up. Looks black.*

Assuming that the reviewer meant Fig. 1, the blue diamonds referenced in the figure caption are outlined in black but filled with blue, which is hopefully clear in the PDF. The updated figure has removed the black outlines.

36. *What are the bin sizes of latitude and SST used to create this plots?*

These are now stated explicitly in the figure caption as 20 degrees latitude and 5 degrees in SST.

20 37. *Captions and discussions of Fig. 2 say Nw but you plotted log10Nw*

These have been changed wherever appropriate.

38. *The satellite is not sensitive to smallest drops, and probably also not to the lowest number concentrations. This seems to explain some of the differences in flat vs. peaked DSD shape in Fig. 2.*

This is indeed discussed later in the manuscript.

25 39. *Evaporation below the lowest altitude of GPM would impact the smallest drops first (see Matthew Kumjian et al. papers with observations and models). So, this effect, if it’s occurring, would eliminate the small drop portion of the spectrum first, most likely. Since small drops usually present in large number concentrations (Thompson et al. 2015, Dolan et al. 2018), this might mean that the satellite also misses large number concentration DSDs as a result of missing the smallest drops.*

30 This is true, but the authors suspect that GPM’s limited sensitivity to small drops and low number concentrations may be the dominant factor.

35 40. *The exponential DSD is the most commonly occurring, which is why large combined or averaged datasets of DSD often exhibit a shape of this kind (explained in Bringi and Chandrasekar 2001). However, this book also states why you wouldn’t expect high- frequency observations of DSD (such as from 1-min observations) to look exponential. The Marshall Palmer was also based on stratiform, steady, UK rain... so again, it’s most representative of this steady-state, averaged, stratiform, weakly-forced rain DSD.*

This is a good point, and factored into our discussion of the histograms from disdrometer observations necessarily looking somewhat different from the large domains observed by GPM.

41. *It is stated on page 10 that rain rate is 3rd moment of DSD; it's actually 3.67th moment. LWC is 3rd moment (Bringi and Chandrasekar 2001).*

5 The text as written reads: "...with the rain rate calculated as the integral product of the velocity distribution and the third moment of  $N(D)$ ." This is correct as stated. Velocity is proportional to  $D^{0.67}$  (Atlas and Ulbrich 1974), which is then integrated in a product with  $D^3$  and other factors.

42. *"Result in a small overestimation of rain rates by 0.06 mm/hr or 1.9%" - unclear how this was calculated? At all rain rates? Or overall error? I'm confused how the error in mm/hr can be just one number?*

10 To see this visually, we can look at a histogram of rain rate differences. This figure was not included as it did not seem a major conclusion of the work, but in the text we just provide the mean difference and point to how for some points, this can be a significant error source in the final calculated rain rate, as originally mentioned in the final section of the manuscript.

43. *Raw observations - it's not really raw. You selected certain sizes, the data have been converted from voltages at fractions of a second to DSD parameters based on A LOT of assumptions contained in the Klepp papers. They are not raw, but they are*  
15 *observations you described already in methods. Just don't use a new qualifier to describe them a different way.*

This is a fair point, and uses of 'raw' have been removed.

44. *How were the "random samples" and "random sampling" and "randomly sampled subsets" performed? Chunks of data taken at random? How much? Explain.*

Every use of the word 'random' in the manuscript means that the Python random function within numpy was used, so cases  
20 taken are effectively random. This means in practice that the authors are not cherry-picking any cases or subsets, but rather taking true random samples.

45. *Page 11: "curve was chosen"... I just see lots of curves on Fig. 5. How was it chosen?*

This has been amended to be more specific: "...chosen, judged by the highest posterior probability."

46. *Last sentence of 4.1 - was this also seen by Dolan et al. 2018?*

25 Indeed it was. We have added the following to conclude that sentence: "... and consistent with findings from Dolan et al. (2018)."

47. *Text at top of Page 12: it seems that you are trying to say that all GMM output DSD fits depart from the exponential form, so that observed mu almost never equals zero.*

Yes, or at least that a pure exponential is not a dominant mode of the distributions observed. To emphasize this point, the  
30 following sentence has been added: "Indeed, the distributions produced by GMM seldom resemble a pure exponential DSD."

48. *Fig. 6 - label legend better in terms of GMM and MGD parameters (and explain in plain language, it's not clear here). In caption, differentiate solid and dashed lines. Water content should be LWC. Keep consistent terminology/abbreviation throughout.*

The caption has been modified to state which lines correspond to GMM and MGD, and 'water content' has been changed to  
35 'RWC.'

49. Page 13: *rare to have -> rare to observe; observations -> minutes*

Done

50. *Last few sentences before Fig. 7 does not make any sense; overly literary and wordy. And it's not clear how these conclusions can be drawn from what is shown.*

5 This section has been trimmed and clarified: "In other words, DSDs featuring a strong peak near  $D_m$ , and for which an exponential is a very poor approximation, are not very common. This can also be seen in Fig. 3, as the PDF is relatively weak in the bottom left of that plot."

51. *It's not clear how interpretation of BIC in Fig. 7 leads to the conclusion made by the authors. I'm totally confused how there can be a singular set... seems like an oxymoron and I don't know what this is intended to mean. It actually appears like 2 modes describe most of the variability (highest BIC) and then Ngmm from 3-6 does fairly and equally well.*

To be clear, the lowest BIC is desirable, as stated in S2.3: "The minimum BIC thus signifies the optimal K value, maximizing the variability explained with the fewest possible classes." And yes, a singular set (or an optimal set) may well be an impossible outcome to expect but that was something we wanted to investigate here, with the conclusion that such a set does not appear to exist or is at least not very clear.

52. *The last paragraph of Sec 4 is very problematic and hard to follow, and hard to deduce the conclusion from the results shown. The claims appear unsubstantiated as written. I don't know what "decoupled from RWC" . . . there was no regional comparison performed. . . use of "not particularly" and "not especially distinct" are handwavy and should be replaced by quantifiable and specific terms.*

This paragraph has been reworked, and the use of adverb qualifiers reduced to clarify these statements. The difficulty in conveying these ideas is that it is inherently not quantifiable that a singular set of DSD shapes does not exist, or that one region or latitude band is not best described by a particular shape, as these are subjective conclusions (though for the latter the plot of BIC provides some evidence). Instead we endeavor to be as specific as possible without overstating our conclusions. With fuller sampling from OceanRAIN these conclusions could be stronger.

53. *What are "variational" systems? Page 14*

54. 'Variational' refers to both retrievals and data assimilation systems that minimize a cost function in an iterative manner, e.g. 1DVAR, 3DVAR, 4DVAR. To make this clear for readers the text has been amended: "...biases in variational systems (e.g. 1DVAR, 3DVAR) if not..."

54. *"Water content" is stated. . . but else where its RWC. stick with consistent terminology/abbreviation once defined, otherwise it sounds like you are introducing a new concept or field.*

55. This has been changed to RWC in all instances.

55. Page 14: *"was used to perform forward model simulations" ... of what? Incomplete sentence.*

It is not an incomplete sentence, and 'forward model simulations' is a common way to refer to radiative transfer. But it has been rewritten: "Forward model simulations of the radiative transfer were performed using the Atmospheric Radiative Transfer Simulator (ARTS) version 2.3 (Eriksson et al., 2011; Buehler et al., 2018)."

56. Page 14: *what are the custom distributions, or habits? Mentioned but not explained sufficiently.*

Amended thus, removing references to habits since we do not use mixed-phase or ice hydrometeors here: "The ARTS model can handle custom particle size distributions (such as observational size bin data) as well as prescribed DSDs such as the MGD."

57. *Unclear what  $g_{m-3}$  cloud looks like or what this number is supposed to represent.*

- 5 This is a cloud liquid water path value, quite common in the remote sensing literature as exemplified by the reference given to Lebsock et al. (2008). Because it is only mentioned once, the authors thought it best to not introduce another acronym (CLWP) and instead give the column mass and depth of the cloud layer. This was similarly done in Duncan et al. (2018).

58. *Define TESSEM2*

Done

- 10 59. *How was the change in TB computed? From level to level or from certain simulations? The description of Fig. 8 and these simulations is very confusing. I don't really know what you are trying to do or how you are doing it. Clarify. What are the units of TB here? What about units of RWP? Units need to be stated in the text. I don't understand what impacts are being tested here, "The 89 GHz shows little impact" . . . impact of what on what?*

- This was computed as the top of atmosphere change relative to RWP of 0, now stated explicitly in the text. TB is given in Kelvin, and its change in  $\Delta K$ , as is standard. "Impact" has been changed to "sensitivity" to be more specific. RWP is given in units of  $\text{kg m}^{-1}$ , now stated explicitly when first introduced.

60. *What do you mean by "largely cancels out its emission signal?" Page 14*

- 20 Radiative transfer impacts are usually referred to in terms of emission signals and scattering signals, in this case positive and negative impacts on measured  $T_B$ . This statement means that the impact on  $T_B$  from scattering is about equal to the impact from increased emission, and so these cancel out. This sentence was slightly modified for clarity: "...its signal is mainly from cloud water emission, and the scattering signal from rain largely cancels out its emission signal from rain."

61. *What are the sizes of cloud droplets and rain droplets that produce these stated differences in emission vs. scattering?*

This information has been added: "Cloud droplets are monodisperse with diameter  $15 \mu\text{m}$ , whereas the rain drops are about two orders of magnitude larger in diameter, hence the differing scattering properties."

- 25 62. *Fig 8 and Fig. 9 and other figures where error bars (of some kind?) are shown - need to define on legend what the errors bars and whiskers and dots really mean.*

It is already stated in the caption of both figures that means and standard deviations are shown. We now state explicitly in the caption that the means are given by dots and the standard deviations by bars.

63. *Add titles to Fig 8 so that you can tell from looking at the plot what the differences between a and b are.*

- 30 Done

64. *Fig. 8 discussion: "net response" should be "mean value" according to your plot. Be specific about what you are discussing. I'm confused what "response" means in this context.*

Here 'net response' has been changed to 'mean value.'

- 35 65. *The averaging window of 6 min seems too short to prove your point. Assume that ships transit at 10 kt (nautical miles per hour) - a good assumption, or you can test it with all the meta data in the ODM dataset. Anyway, figure out how long in*

time you need to average in order to approximate a 5 km or degree or whatever distance spanned by a single pixel of satellite data

So, 10kt is 18.52kmph, so it would take about 16min to traverse a 5km distance at that speed. The data have been reanalyzed using this time window, and the figure updated: "Specifically, a nominal 16 minute window was used to average consecutive raining disdrometer measurements, in that a ship at 10 kn would take about 16 minutes to traverse 5 km."

66. "Should not be markedly different." . . . If what? Compared to what? A comparison or warning seems to be made, but it's not clear what it is.

The language here has been amended: "The maximum forward model errors observed by a sensor such as GMI may not be markedly different than those presented with the time averaging performed, however most GMI channel footprints are larger than that of DPR."

67. "Non-raining points" – do you mean that you did not average zero values? Unclear

This has been clarified: "Observations with zero rain rates.."

68. Fig. 9 - why aren't data shown above 40 mm/h? Surely they exist in ODM?

This figure has been extended up to now include the largest bin at  $46 \text{ mm h}^{-1}$ . The data become noisy at the higher rain rates due to a low sample size (the final bin shown contains only 17 observations), and this is now noted in the text as well.

69. The author's conclusion that the error is way bigger for the blue line is not well- supported. The errors are only different in blue v. red at the very highest rain rates (above 10 mm/hr). Consider revising interpretations for clarity / consistency.

In fact, the standard deviations shown at  $K_A$  are smaller at every single rain rate shown. They may not be much different at the lower end, but they are still smaller.

70. Page 16 "largely been predicated on limited land-based observations in the past" - including some island observations from Manus, Gan, and Kwajalein.

The key word here is 'largely' and this seems to be true.

71. Page 16: here it is stated that DSD have limited dependence exists on SST, but in presentation of Fig. 1 you remarked that there appeared to be an SST dependence. Inconsistent.

This is consistent, because despite there being some dependence, it is indeed quite limited.

72. Page 16 in several places: datasets "observe" -> exhibit. Not literally true.

Changed

73. Summary and Conclusions: your latitude bands are very wide and may inhibit your ability to draw conclusions about DSD variability that could be present in regimes such as the monsoon, ITCZ and SPCZ, subtropical highs, western boundary currents that are really warm, cold current regions, etc.

To check this, this figure was remade with tighter latitude bands, seen below. The conclusions do not really change, but some bands are much more sparsely populated:

74. "Function to encapsulate" and "appears more applicable" –> unclear. Revise.

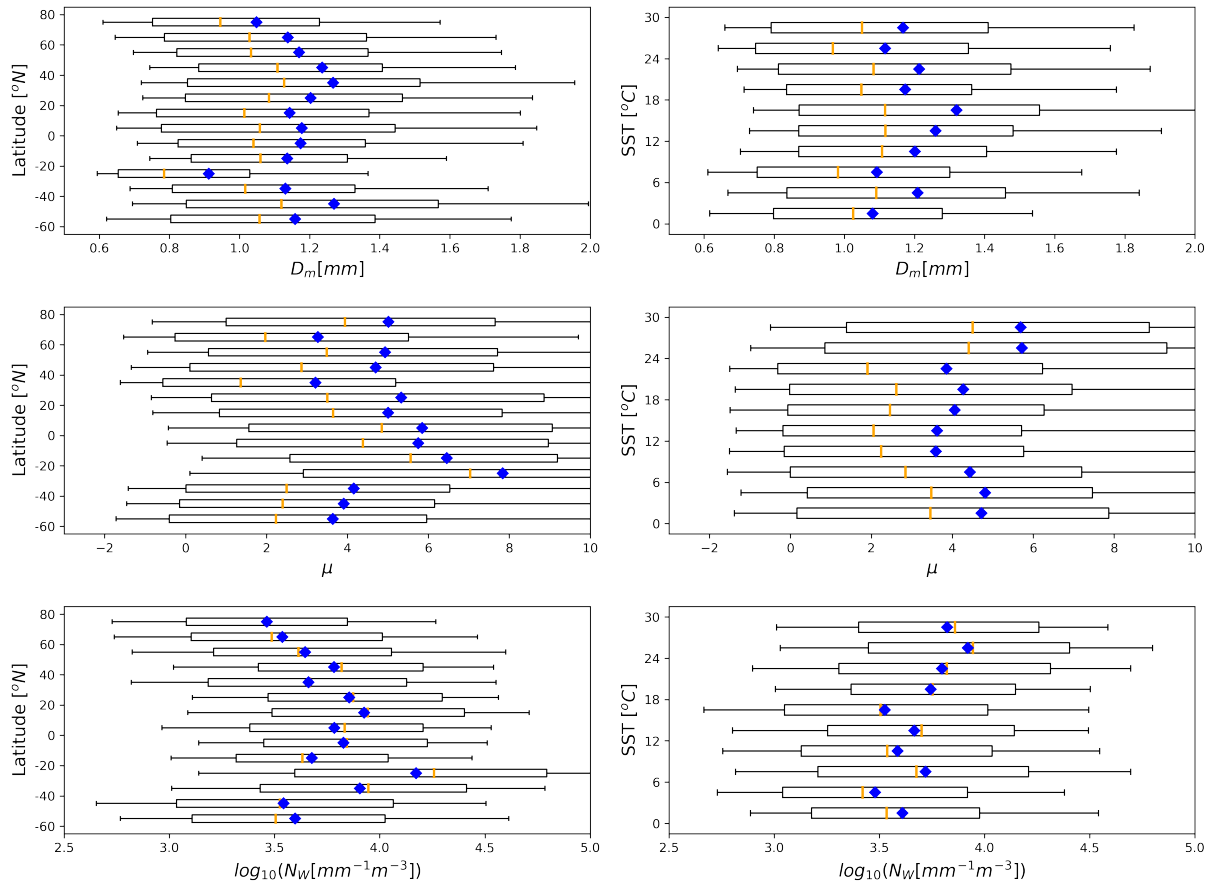


**Figure 1.** As in Fig. 1 of the original manuscript (now Fig. 2), but with tighter latitude and SST bins.

Revised thus: "Usage of the normalized gamma function to describe all observed DSD behavior was questioned, as it appears more applicable in the Tropics than for higher latitude populations, as high latitude cases exhibit larger concentrations of small drops that are outside the state space specified by the 3-parameter MGD (Fig. 11)."

75. Line 3 page 17: *spatial and temporal considerations*

5 Done

76. Unclear what this sentence means "Its use can cause systematic. . ."

This has been revised: "The 3-parameter MGD can cause systematic biases in rain rate estimation relative to using the observed size bin data, quantified to be a -2% error in the mean relative to total accumulation calculated from the disdrometers."

77. Sentence with "for about 3% of cases . . ." = run-on sentence. Revise to simplify it.

10 The comma has been replaced by a semicolon.

78. Page 17 lines 12-24 make very little sense. Revise for clarity a. Uncertainty = standard deviation? Width of distribution? means? b. What is "radiative uncertainty"? c. How "rapidly" d. What is meant by low vs. high frequencies? e. "Half the

- radiative signal” - do you mean the mean? f. What is “true for passive and active simulations” ?? unclear based on what has been shown or discussed g. Unclear why “retrieving the DSD would shrink these ranges” unsupported from what is shown or explained, or maybe it just doesn’t make sense h. Lines 19-24 don’t really make any sense. Revise. Unclear. i. It’s confusing that you bring up dewpoint temp and RWC on line 28 because you didn’t discuss Td anywhere else but you did use RWC.*
- 5 *j. What is meant by “limited spatiotemporal sampling of OceanRAIN”? – Please include a map in the revised manuscript k. What references can you provide to justify why DSDs are more uniform over land. They seem to exhibit more modes over land because hail and mixed-phase and very intense convective microphysical processes can occur. Unclear from what is written.*
- This section has been significantly modified to use more exact language.

## References

- Buehler, S. A., Mendrok, J., Eriksson, P., Perrin, A., Larsson, R., and Lemke, O.: ARTS, the Atmospheric Radiative Transfer Simulator – version 2.2, the planetary toolbox edition, *Geosci. Model Dev.*, 11, 1537–1556, <https://doi.org/10.5194/gmd-11-1537-2018>, 2018.
- Dolan, B., Fuchs, B., Rutledge, S. A., Barnes, E. A., and Thompson, E. J.: Primary Modes of Global Drop Size Distributions, *J. Atmos. Sci.*, 5 75, 1453–1476, <https://doi.org/10.1175/JAS-D-17-0242.1>, 2018.
- Duncan, D. I., Kummerow, C. D., Dolan, B., and Petković, V.: Towards variational retrieval of warm rain from passive microwave observations, *Atmos. Meas. Tech.*, 11, 4389–4411, <https://doi.org/10.5194/amt-11-4389-2018>, <https://www.atmos-meas-tech.net/11/4389/2018/>, 2018.
- Eriksson, P., Buehler, S., Davis, C., Emde, C., and Lemke, O.: ARTS, the Atmospheric Radiative Transfer Simulator, version 2, *J. Quant. Spectrosc. Radiat. Transfer*, 112, 1551–1558, <https://doi.org/10.1016/j.jqsrt.2011.03.001>, 2011.
- Klepp, C.: The oceanic shipboard precipitation measurement network for surface validation — OceanRAIN, *Atmos. Res.*, 163, 74 – 90, <https://doi.org/https://doi.org/10.1016/j.atmosres.2014.12.014>, <http://www.sciencedirect.com/science/article/pii/S0169809515000034>, 6th Workshop of the International Precipitation Working Group, 2015.
- Klepp, C., Michel, S., Protat, A., Burdanowitz, J., Albern, N., Kähnert, M., Dahl, A., Louf, V., Bakan, S., and Buehler, S. A.: 15 OceanRAIN, a new in-situ shipboard global ocean surface-reference dataset of all water cycle components, *Sci. Data*, 5, 180 122, <https://doi.org/10.1038/sdata.2018.122>, 2018.
- Lebsock, M. D., Stephens, G. L., and Kummerow, C.: Multisensor satellite observations of aerosol effects on warm clouds, *J. Geophys. Res. Atmos.*, 113, <https://doi.org/10.1029/2008JD009876>, 2008.
- Thurai, M. and Bringi, V. N.: Application of the Generalized Gamma Model to Represent the Full Rain Drop Size Distribution Spectra, *J. Appl. Meteorol. Climatol.*, 57, 1197–1210, <https://doi.org/10.1175/jamc-d-17-0235.1>, 2018.
- 20

# On the distinctiveness of observed oceanic raindrop regimes distributions

David Ian Duncan<sup>1</sup>, Patrick Eriksson<sup>1</sup>, Simon Pfreundschuh<sup>1</sup>, Christian Klepp<sup>2</sup>, and Daniel C. Jones<sup>3</sup>

<sup>1</sup>Department of Earth, Space, and Environment, Chalmers University of Technology, SE 412 96 Gothenburg, Sweden

<sup>2</sup>ClISAP/CEN, Meteorological Institute, Universität Hamburg, 20146 Hamburg, Germany.

<sup>3</sup>British Antarctic Survey, CB3 0ET Cambridge, United Kingdom

**Correspondence:** David Ian Duncan (david.duncan@chalmers.se)

**Abstract.** Representation of the drop size distribution (DSD) of rainfall is a key element of characterizing precipitation in models and retrievals, with a functional form necessary to calculate the precipitation flux and the drops' interaction with radiation. With newly available oceanic disdrometer measurements, this study investigates the validity of commonly used DSDs, potentially useful a priori constraints for retrievals, and the forward model ~~errors caused by impacts of~~ DSD variability.

5 These data are also compared ~~to~~ with leading satellite-based estimates of oceanic DSDs, indicating that the disdrometers observe more small drops and more variable number concentrations. Forward model errors due to DSD variability are shown to be significant for both active and passive sensors. The modified gamma distribution is found to be generally adequate to describe rain DSDs, but may cause systematic errors for high latitude or stratocumulus rain retrievals; depending on the application, an exponential or generalized gamma function may be preferable for representing oceanic DSDs. An unsupervised  
10 classification algorithm finds a variety of DSD shapes that differ from commonly used DSDs, but does not find a singular set that best describes the global variability. ~~Finally, DSD shapes are found to be not particularly distinctive of regional or large-scale environments, but rather occur at varying frequencies over the global oceans.~~

## 1 Introduction

A challenge shared by atmospheric models and remote sensing retrievals alike is the representation of precipitation micro-  
15 physics. Raindrops can be modeled using a variety of functional forms, simple relations between drop size and number density that attempt to capture the ~~bulk overall~~ behavior in a way sufficient to represent the processes of interest. The radiative characteristics and precipitation flux through an atmospheric volume containing precipitation depend on the size and resulting terminal velocities of the rain drops, defined via that volume's drop size distribution (DSD). In this way, the DSD acts as a necessary conduit to represent precipitation processes, one common to climate models, radar retrievals, and data assimilation  
20 schemes.

Various functional forms have been employed to describe rain DSDs. Exponential DSDs (Marshall and Palmer, 1948) have been ~~common used~~ in radar meteorology for decades, and different versions of the modified gamma distribution (MGD; Eq. 1) have gained popularity for remote sensing (Ulbrich, 1983). Simplifications of the MGD to three, two, or single parameter versions yield the gamma, exponential, and power law relations (Petty and Huang, 2011), respectively, all of which are used

to represent DSDs in various applications. Note that the four parameter MGD is sometimes called the generalized gamma distribution (Petty and Huang, 2011; Thurai and Bringi, 2018). Between those who use the MGD to describe DSDs, disagreement exists on how many free parameters to use (Smith, 2003; Thurai and Bringi, 2018), whether it is best to normalize the distribution (as in Eq. 3) in some way (Testud et al., 2001), or if the separation of parameters in the MGD is either physically meaningful or outperformed by simpler methods (Williams et al., 2014; Tapiador et al., 2014).

The below equations will be referred to throughout the text as the generic MGD function (Eq. 1) and normalized gamma (NG) function (Eq. 3), with NG a normalized and 3-parameter version of the MGD. Here  $N(D)$  is the number of drops per volume per size as a function of the drop diameter,  $D$  (with  $D$  given in mm and  $N(D)$  in  $\text{mm}^{-1} \text{m}^{-3}$ ). The so-called shape parameter is  $\mu$  while  $N_0$  and  $N_w$  are intercept parameters and  $\mu$  is the shape parameter, though, with  $N_w$  is (Eq. 5) a normalized intercept parameter.  $D_m$  is the scaled by the water content (Testud et al., 2001). The mass-weighted mean diameter is  $D_w$  (Eq. 2), the ratio of the fourth and third moments of the distribution (Eq. 2).  $\Gamma$  is Denoting the gamma function is  $\Gamma$ ,  $\rho_w$  is the density of water, and  $RWC$  is the rain water content in  $\text{kg m}^{-3}$ .

$$N(D) = N_0 D^\mu e^{-\lambda D^\gamma} \quad (1)$$

$$D_m = \frac{\int_0^\infty N(D) D^4 dD}{\int_0^\infty N(D) D^3 dD} \quad (2)$$

$$N(D) = N_w f(\mu) \left(\frac{D}{D_m}\right)^\mu e^{-(4+\mu)\frac{D}{D_m}}, \quad f(\mu) = \frac{\Gamma(4) (4+\mu)^{4+\mu}}{4^4 \Gamma(4+\mu)}, \quad N_w = \frac{4^4 RWC}{\pi \rho_w D_m^4} \quad (3)$$

$$f(\mu) = \frac{\Gamma(4) (4+\mu)^{4+\mu}}{4^4 \Gamma(4+\mu)} \quad (4)$$

$$N_w = \frac{4^4 RWC}{\pi \rho_w D_m^4} \quad (5)$$

Scattering of radiation is highly dependent on particle size, and thus the DSD is a crucial component of remote sensing retrievals, whether it is assumed or retrieved. Depending on the application, the specific choice of DSD may or may not make much difference (e.g. Smith (2003); Illingworth and Blackman (2002)). (Smith, 2003; Illingworth and Blackman, 2002). For instance, erroneous assumptions about small drops may not impact the bulk broadband radiative fluxes or precipitation characteristics of a volume, but a more accurate DSD representation may be necessary when considering additional frequencies or polarized measurements. The under-constrained nature of precipitation retrieval means that the DSD is either assumed completely or needs to be quite constrained to allow tractable solutions.

A lack of ~~globally representative global~~ DSD data has hampered the retrieval of precipitation from satellites. Satellite retrievals rely heavily on a priori knowledge to constrain the solution space, and regional differences in meteorology and microphysics can manifest as regional biases in satellite retrievals (Berg et al., 2006). Whereas ground radar networks and arrays of disdrometers over land have helped to characterize the variability of raindrops from continental precipitation (~~e.g. Bringi et al. (2003); Williams and Gage (2009); Thurai and Bringi (2018)~~)(Bringi et al., 2003; Williams and Gage, 2009; Thurai and Bringi), observations of DSDs over ocean have mostly been limited to field campaignsand, a few small tropical islands and atolls, and coastal radar retrievals. Because of the different aerosol loading, convective strength, and underlying humidity of airmasses over land, oceanic drop populations can be ~~quite~~ distinct from those over land (Dolan et al., 2018), with the different microphysics influencing satellite retrievals(~~Petković et al., 2018~~). It is thus desirable to have measurements of DSDs over ocean, and crucial that these measurements are globally representative rather than skewed toward one region or another.

It is expedient to condense the variability of DSDs into a few distinct classes, either to narrow the possible solution space of remote sensing retrievals or for interpretation of results. Separation of stratiform and convective precipitation has long been common, as stratiform precipitation tends to have a more peaked distribution of fewer, smaller drops versus the more exponential distribution of precipitation from convective clouds (Thurai et al., 2010; Thompson et al., 2015). However, partitioning stratiform and convective rainfall is done in various ways and may differ depending on location. A little further, Dolan et al. (2018) argue for six dominant modes of DSDs globally, separated via principal component analysis but linked to meteorology and attendant microphysical regimes. As many studies of drop distributions are from land-based disdrometers and radars, DSD variability has been studied less over open ocean where a majority of global precipitation occurs, though advances are being made in this area (Thompson et al., 2018).

In remote sensing applications, one can attempt to solve for all, some, or none of the parameters that define a functional form such as Eq. 1, depending on the information content available. A normalized distribution such as Eq. 3 is used in many precipitation retrievals to separate the water content from the spectrum's shape. In that formulation with RWC separate, this leaves two free parameters to define the distribution since RWC is directly related to  $N_w$  through  $D_m$ . While passive-only retrievals may need to assume one of these parameters because of the limited signal available (Duncan et al., 2018), radar or combined radar/radiometer retrievals may solve for these parameters in a constrained way (Munchak et al., 2012; Grecu et al., 2016). Precipitation retrievals thus handle the complexity of the DSD differently depending on their ~~sensitivity instruments'~~ sensitivities, but necessarily using a predefined functional form to limit the inverse problem's degrees of freedom.

To investigate the distinctiveness of raindrop ~~shape regimes size distributions~~ over the global oceans, and how ~~these regimes~~ this may impact retrievals both in terms of prior constraints and radiative transfer modeling, the study proceeds as follows. Data and methods are described in the next section, introducing the disdrometer and satellite data examined, as well as the machine learning technique used to classify drop regimes. Section ~~3~~ 3 presents a holistic view of global disdrometer measurements with respect to the normalized gamma distribution, including a comparison to the leading satellite-based, near-global DSD data set. ~~Section 4 critically examines the disdrometer data versus a commonly used functional form and investigates how distinct raindrop regimes truly are~~ Results from the application of a machine learning technique to the disdrometer data are discussed in Section 4. In Section ~~5~~ 5 the radiative aspects of DSD variability are addressed in the context of satellite retrievals with

radiative transfer modeling. Then follows a discussion section, critically examining the disdrometer data versus a commonly used functional form. The paper closes with a summary and some conclusions.

## 5 2 Data and Methods

### 2.1 OceanRAIN

The Ocean Rainfall And Ice-phase precipitation measurement Network (OceanRAIN) coordinates disdrometer measurements and acquired ancillary data aboard research ships across the global oceans (Klepp et al., 2018). The data set begins in 2010 and collection is ongoing, with observations spanning 8 vessels and over 6 million minutes covering all ocean latitudes. OceanRAIN data contain raw counts integrated for each minute of rain, snow, or mixed-phase precipitation, with derived rainfall DSD parameters ~~fitting~~ (Eq. 3), and various ancillary fields. The large and growing size of the data set make statistical analysis possible due to its consistent application across various ships. The ~~raw~~-disdrometer data are integrated per minute and separated into logarithmically-spaced size bins (Table 1), permitting analysis of DSDs without the assumption of a functional form. Specifically, the OceanRAIN-M (“OceanRAIN Microphysics”) data are used primarily in the study (Klepp et al., 2017), in which ~~raw~~-drop counts from the disdrometer are converted to number concentrations per size (i.e. drops per volume per size), the form in which DSDs are ~~commonly-often~~ given. DSD assumptions commonly made in the literature can thus be assessed against the ~~unmolested~~-observations.

Underpinning OceanRAIN is the ODM470 optical disdrometer, a sensor with sensitivity to hydrometeors of diameter ~~0.3-0.4~~ to 22 mm (Klepp, 2015). The disdrometer is deployed on the superstructure of ships in a package including a cup anemometer and a precipitation detector to activate the disdrometer. A wind vane turns the disdrometer to keep the optical path normal to the wind direction, and the disdrometer’s cylindrical volume ensures that the incident angle of hydrometeors does not affect the measurement. These work in concert to minimize impacts of turbulence from local up- and down-drafts, to limit under-catchment and drops impacting the sensor from various directions (Klepp, 2015). Only data points marked as rain definite, with 50 or more measured drops, and with a probability of precipitation of 100% were used in the following analysis. To be consistent, only data points with measurements in ten or more size bins are used (Klepp et al., 2018), as these provide the parameters from the NG fit to Eq. 3. A visualization of the OceanRAIN sampling used in this study is found in Fig. 1, with raining minutes shown on a near-global regular grid.

This study also makes use of simulated reflectivities in Section 5. Simulated reflectivities from the ODM470 disdrometer have demonstrated high correlation and a near-zero bias when compared against co-located, vertically-oriented radar observations (~~see Fig. 6, Klepp et al. (2018)).~~ (Klepp et al., 2018, Fig. 6). In comparisons with co-located rain gauges, the optical disdrometer performs better in high wind speeds, as ~~undercatch-under-catch~~ is a significant problem for traditional rain gauges that can result in underestimation of rainfall accumulation by 50% (Grossklaus et al., 1998; Klepp et al., 2018), though accumulations match within 2% for low wind speeds (Klepp, 2015). The ODM470 has been used in a variety of conditions and shown no difference in accuracy between oceanic and continental cases (Bumke and Seltmann, 2011).

~~The robustness-~~

**Table 1.** Center drop diameters for OceanRAIN size bins, given in mm. Note that the bins of up to 5 mm diameter are given here for brevity and because these bins contain the vast majority of drop counts, but larger size bins also exist. The values are rounded to 3 digits. For full details see Klepp et al. (2017).

.392	.427	.462	.498	.535	.573	.612	.652	.693	.735
.778	.823	.868	.914	.961	1.01	1.06	1.11	1.16	1.22
1.27	1.33	1.39	1.45	1.51	1.57	1.63	1.70	1.76	1.83
1.90	1.97	2.05	2.12	2.20	2.28	2.36	2.45	2.53	2.62
2.71	2.80	2.89	2.99	3.09	3.19	3.30	3.40	3.51	3.62
3.74	3.86	3.98	4.10	4.23	4.36	4.49	4.62	4.76	4.91

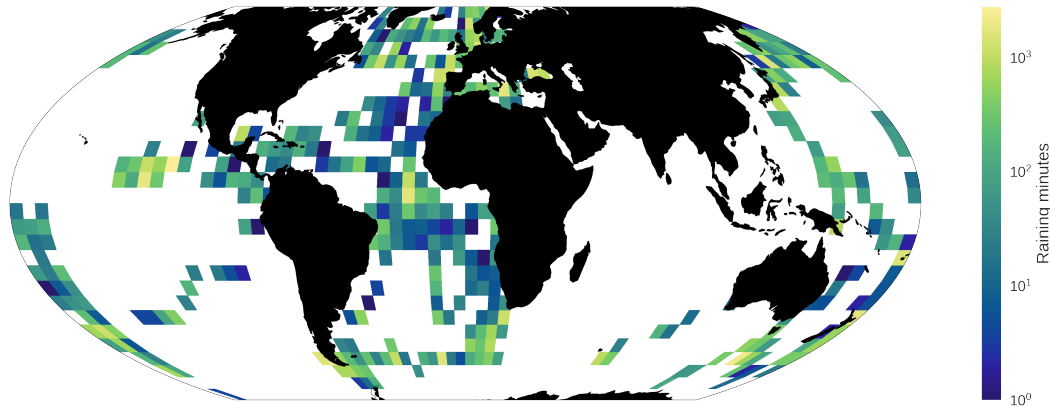


**Figure 1.** Raining minutes from OceanRAIN, selected by the sampling criteria of this study as described in Section 2.2, viewed on a regular  $5^\circ$  grid. Grid cells in white signify that no data points were used.

The accuracy of disdrometer-derived DSD parameters (following Eq. 3) will depend somewhat on the parameter discussed and the type of rain. For instance, derived  $D_m$  should be ~~very robust~~ accurate for all but the ~~very~~-weakest rain rates as it is simply defined (Eq. 2) and requires no fitting. The accuracy of derived  $N_w$  may be suspect for cases with high rain rates and a low  $D_m$  value, as drops below the sensitivity threshold ~~of 0.39 mm~~ may constitute a non-negligible fraction of total drops, though this depends on the type of rainfall and is an issue faced by all disdrometers (Thurai et al., 2017). To be clear, there can be significant number concentrations below this sensitivity limit, but voltages corresponding to drop diameters of less than 0.36 mm are disregarded as these can be contaminated by vibrations from the ship (Klepp et al., 2018) and this is a key drawback of the data set. The derived shape parameter,  $\mu$ , is the least ~~robust~~ reliable of the three as it depends on a curve fitting which may not be optimal for ~~very~~-light rain rates or spectra that do not conform to the expected general shape. In other words, the accuracy of DSD parameters reported by OceanRAIN may exhibit bias in regimes with many drops below the disdrometer's sensitivity threshold, or for distributions with a shape unlike that assumed.

In this study, the default way of discussing the OceanRAIN data is using the 3-parameter normalized gamma distribution (Eq. 3), but a strength of this data set is that number concentrations are provided for every observed size bin (Table 1), allowing investigation of different DSD types, including other varieties of the MGD. Later in the study the 3-parameter MGD (i.e. NG, as all DSDs discussed are normalized) is contrasted with 1- and 2-parameter MGD versions as well as DSDs not conforming to the MGD but instead derived from a machine learning technique. In the context used here, the 1-parameter MGD is equivalent to single moment microphysics in model parlance, with a fixed shape (i.e. prescribed  $D_m$  and  $\mu$ ) and  $N_w$  simply scaling with  $RWC$ . The 2-parameter MGD is defined by a calculated  $D_m$  (via Eq. 2) but a prescribed  $\mu$ , whereas the 3-parameter MGD includes calculated  $D_m$  and  $\mu$ , with  $N_w$  determined via  $D_m$  and  $RWC$  (Eq. 5).

## 2.2 GPM Combined Radar-Radiometer Algorithm

The Global Precipitation Measurement (GPM; Hou et al. (2014)) Core Observatory (Hou et al., 2014) holds two sensors designed to measure precipitation: the GPM Microwave Imager (GMI) and the Dual-frequency Precipitation Radar (DPR). GMI is a passive microwave radiometer measuring from 10 to 190 GHz and the DPR is a phased array radar measuring at  $K_U$  and  $K_A$  bands (13.6 and 35.5 GHz, respectively). The dual frequencies of DPR set it apart from other satellite-borne sensors as far as the capacity to solve for the DSD. The GPM core satellite's combination of passive and active sensors provides sensitivity to a large range of precipitating hydrometeors, with information on their emission and scattering characteristics. However, DPR has limited sensitivity to small drops and low number concentrations due to its minimum detectable signal of 12 to 13dBZ.

The GPM ~~combined algorithm (Grecu et al., 2016)~~ Combined Radar-Radiometer Algorithm (Grecu et al., 2016), hereafter referred to as GPM CORRA, is a retrieval that uses data from both radar and radiometer to solve for profiles of hydrometeors that optimally fit the observations. As the GPM ~~core-observatory-satellite~~ represents the best observational platform yet flown for measuring near-global precipitation, the combined retrieval from DPR and GMI is included in this study as the state of the art for calculating global DSD statistics. Via the same DSD formulation given in Eq. 3, the ~~combined retrieval~~ GPM CORRA first uses the  $K_U$  band reflectivities to solve for the  $D_m$  profile. It then retrieves  $N_w$  at a reduced vertical resolution to match the  $K_A$  band ~~and deconvolved reflectivities~~, DPR path integrated attenuation, and ~~de-convolved~~ GMI brightness temperatures ( $T_{BS}$ ) using optimal estimation. The shape parameter is fixed at  $\mu = 2$  for all cases. For further details about this retrieval, see Grecu et al. (2016).

In this study, gridded level 3 GPM ~~Combined-CORRA~~ data are used (Olson, 2017), ~~comprising monthly and daily files from GPM version V06~~. This data set provides statistics of pixel-level derived DSD parameters from Eq. 3 at  $5^\circ$  and  $0.25^\circ$  horizontal resolution. The values used in this study are from the lowest altitude bin and include oceanic pixels only so as to best match the ~~ground-based surface-based~~ data from OceanRAIN-M. Because GPM ~~Combined-CORRA~~ receives most of its information content from DPR, the DSD parameters derived are representative of individual segments of the atmospheric column and not a column average, a key difference from passive-only retrievals. This is significant, as comparison with ~~ground-based observations surface-based observations (Petersen et al., in press)~~ should be as close in altitude as possible, as DSDs will vary with altitude as evaporation, coalescence, collisions, or other processes modify the spectra (Williams, 2016). The 250 m vertical resolution of DPR means that multiple observations exist below 1 km altitude, though some of these will be affected by ~~ground~~

surface clutter and so the lowest bin without clutter is chosen here. Note that the GPM ~~Combined-CORRA~~ retrievals were performed at the native DPR pixel size, which has a 5 km horizontal resolution.

To assess the similarity between GPM estimates and the in situ disdrometer measurements of OceanRAIN, in Section 3.1 the retrieved results for  $N_w$  and  $D_w$  are compared, as GPM CORRA assumes a constant  $\mu$  value. To perform this comparison, level 3 GPM CORRA data were used, spanning 12 months from 2017. Due to the uneven sampling of the ship-borne disdrometers, GPM data included in the analysis are from months with valid OceanRAIN data points in each box and defined as ocean pixels by DPR. No attempt was made to match observations exactly in space and time due to the difficulty of point-to-area comparisons with ship-borne data and GPM (Burdanowitz et al., 2018; Loew et al., 2017).

## 10 2.3 Gaussian Mixture Modeling

Gaussian Mixture Modeling (GMM) is an unsupervised, probabilistic classification technique that attempts to represent a data set using a linear combination of multidimensional Gaussians in a chosen parameter space (Pedregosa et al., 2011). The dimensions (or “features”) of the parameter space and the maximum number of classes,  $N_{GMM}$ , are set by the user. GMM assigns each data point to the class, represented by a multidimensional Gaussian function, with the highest posterior probability for that data point. For further technical details on GMM and its use in other Earth science applications, see Maze et al. (2017) and Jones et al. (2019). ~~The Python package *scikit-learn* supplied the GMM code (Pedregosa et al., 2011).~~

GMM ~~easily~~ generalizes to a wide variety of data distributions and can thus identify structures in the DSD data that might be missed by more traditional curve-fitting-classification methods. This frees the analysis from explicit assumption of a DSD shape such as Eq. 3. In the approach used here, the ~~“dimensions”~~ dimensions given to the GMM module are the size bins used by the OceanRAIN disdrometers and thus the input data are an array of approximately 90000 raining minutes with 60 size bins. These data are unchanged other than being normalized so that DSD “shape” variability in the data set is not weighted by the total number of drops observed, and cut off at 60 size bins as very few drops over 5 mm are ever measured. Because the shapes are independent of the total number of drops, this is analogous to the normalized DSD approach typified by Eq. 3. GMM thus finds common shapes of the observed DSDs and determines the posterior probability of ~~each~~ every data point (DSD for each raining minute) falling into each of the various classes. Each observed DSD is assigned to the GMM class for which it has the highest posterior probability. The resultant classes provide insight into dominant structures of the input data, with this approach exemplified in Section 4.

The number of GMM classes is set a priori, with the degree of complexity described by the GMM decomposition dependent on the number of states set by the user. Determining an optimal value for  $N_{GMM}$  is thus important but somewhat subjective because the desired level of complexity retained after the decomposition will vary for different applications. One method for estimating a suitable range for the number of classes is to use the Bayesian Information Criterion (~~BIC~~; Schwarz, 1978). Shown in Eq. 6. ~~This metric~~, this metric (BIC) contrasts the log likelihood (L) against a cost for the number of classes (K) to provide an objective measure of how many classes should optimally describe the data, where  $N_f(K) = K - 1 + KD + KD(D - 1)/2$ , with  $D$  the dimension of the data space and  $n$  the number of data points used in model training. The first term in Eq. 6 becomes more negative with increased likelihood, while the second term acts to penalize overfitting. The minimum BIC thus signifies

the optimal K value, maximizing the variability explained with the fewest possible classes. A plateau of BIC values versus K would signify no distinctly optimal K to describe the data's variability, but rather a range of solution spaces in which the addition of further states provides marginal additional complexity.

$$BIC(K) = -2L(K) + N_f(K)\log(n) \quad (6)$$

## 10 3 Global ~~DSD-observations~~results

### 3.1 Disdrometer ~~data~~results

Viewing the OceanRAIN data all together can provide a sense of the variability in DSD populations over the world's oceans. From the perspective of global retrievals, constraints on the DSD that depend on the location or environmental regime, rather than, say, partitioning stratiform and convective precipitation a priori, are useful for independent satellite-based products that do not ingest detailed model data, such as the operational retrievals for the GPM constellation radiometers (Kummerow et al., 15 2015). To this end, the derived parameters of Eq. 3 are given for all raining disdrometer observations, separated by latitude and SST in Fig. 2 ~~and representing all data points shown in Fig. 1~~. As this is the DSD form most used in rainfall retrievals currently, it is presented here.

As seen in Fig. 2, the normalized gamma DSD parameters exhibit a wide range of variability that is not strongly tied 20 to ~~location~~latitude or SST. The strongest trend visible is that higher number concentrations occur over warmer ocean surfaces ~~witness greater densities of drops~~, with the mean  $\log_{10}(N_w)$  increasing from about 3.5 to 4.0, as may be expected due to the Clausius-Clapeyron equation. This is roughly in line with the a priori  $N_w$  used for rain by Mason et al. (2017) of  $3.9e3$ , or 3.59 in log space. It is noted that the distributions of  $D_m$  and  $\mu$  are not ~~particularly~~-Gaussian, with the means and medians separate, and  $N_w$  only moderately Gaussian in log space.

25 It is stressed that OceanRAIN observations are not evenly distributed around the global oceans and thus the values seen are dependent on the sampling (i.e. where the ships sailed, see Fig. 1), so these values are not fully representative of each ocean latitude band. As surface-based observations, they do not provide information as to any vertical DSD variability, a topic that requires radar observations (Williams, 2016). However, it is possible to pick out some meteorological regimes of interest from the derived DSD parameters in OceanRAIN. For instance, the ships' heavy sampling of Southern Hemisphere stratocumulus 30 regions (Fig. 1 shows up in these plots as a regime characterized by a higher number of small drops and a more peaked distribution (seen in the 20°S to 40°S band in Fig. 2). From the perspective of satellite rainfall retrievals, such location- or cloud regime-dependent a priori constraints are much preferable to a global prior and useable within existing algorithms.

### 3.2 ~~Comparison to GPM~~

~~As mentioned in Section 2.2, GPM is the best satellite-borne platform currently available for measuring DSD variability, and 5 thus the best near-global observational DSD data set for comparison. To assess the similarity between GPM estimates and~~

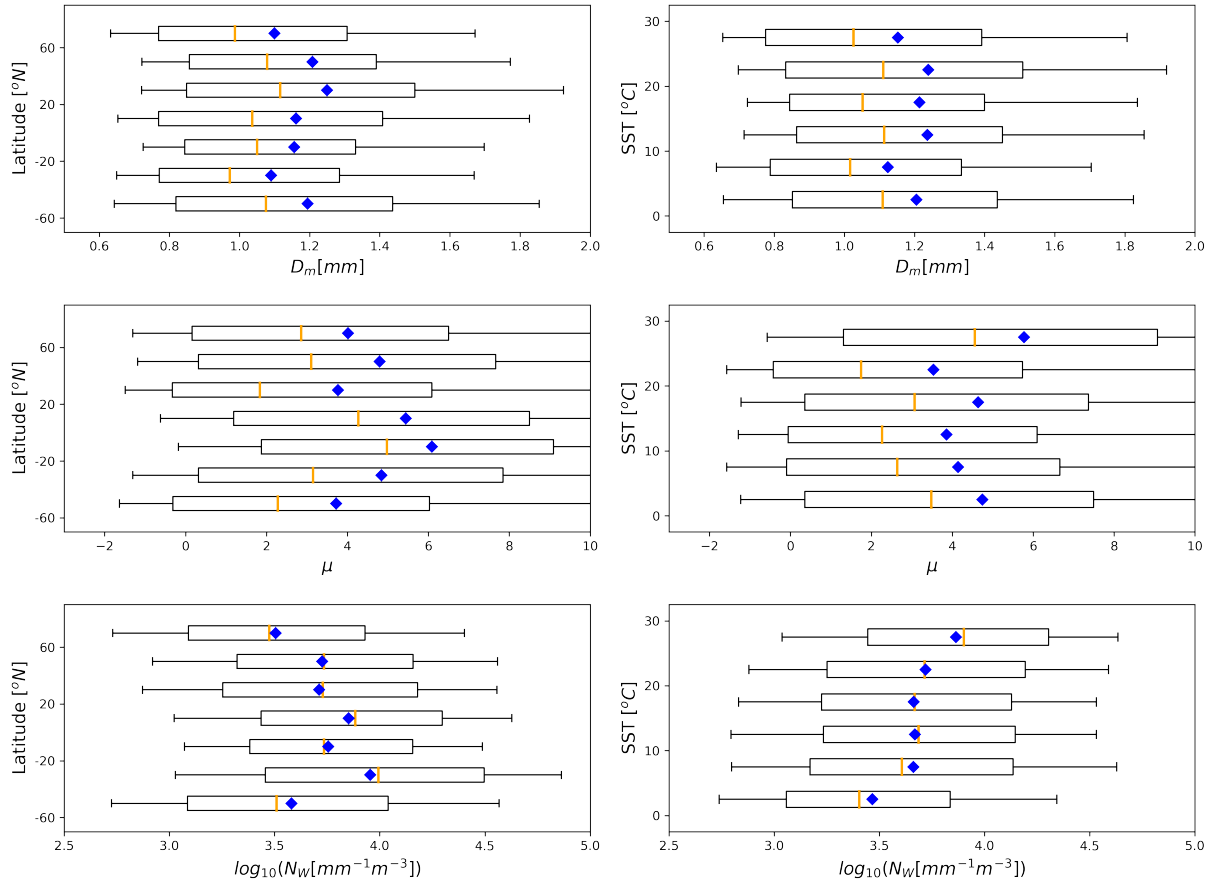


**Figure 2.** Distribution of DSD parameters following Eq. 3. The boxes define the standard deviations ( $\pm 1\sigma$ ), the whiskers define the 10% and 90% bounds, orange lines denote the median, and blue diamonds the mean. Observations are divided according to latitude with  $20^\circ$  bins (left) and sea surface temperature with  $5^\circ\text{C}$  bins (right).

the in-situ disdrometer measurements of OceanRAIN, here the retrieved results for  $N_w$  and  $D_m$  are compared, as the GPM retrieval assumes a constant  $\mu$  value. To perform this comparison, histograms of level 3 GPM Combined data at  $5^\circ$  resolution were used, spanning 12 months from 2017. Due to the uneven sampling of the ship-borne disdrometers, the only GPM data included in the analysis are from months with valid OceanRAIN data points in each box and defined as ocean pixels by DPR. No attempt was made to match observations exactly in space and time due to the difficulty of point-to-area comparisons with ship-borne data and GPM (Burdanowitz et al., 2018; Loew et al., 2017).

The left panel of Fig. 5 shows histograms of derived  $D_m$  from the disdrometers compared with GPM Combined, separated by latitude. Given the limited sensitivity of DPR to small drops, it is unsurprising to note that OceanRAIN observes a wider distribution of  $D_m$  that is most noticeably distinct from GPM results for small drops. Another key feature of these histograms is that while the maxima in  $D_m$  distributions are relatively similar for the two data sets, OceanRAIN observes a much less

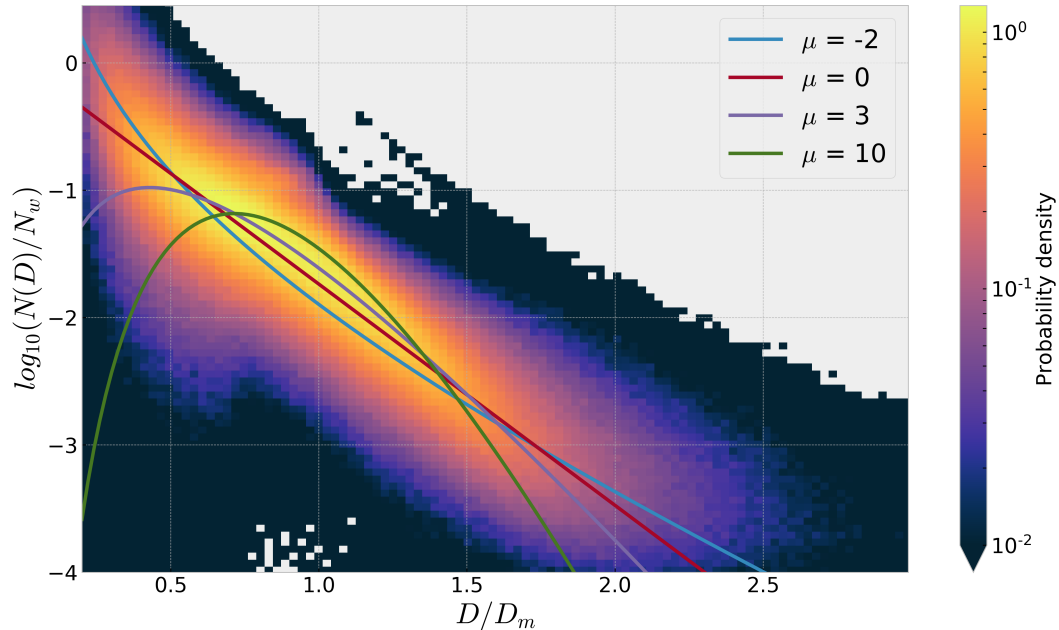


**Figure 3.** Histograms Probability density function of  $D_m$  (left) and  $N_w$  (right) for GPM Combined and all raining OceanRAIN data points, separated visualized using the scaled DSD,  $N(D)/N_w$ , against the diameter normalized by latitude  $D_m$ . GPM data Various curves with prescribed  $\mu$  values are from the 3B-CMB monthly gridded product plotted for comparison. Areas in gray indicate no data.

peaked distribution with a longer tail for larger drops in most latitudes. In the  $40^\circ$  to  $60^\circ$  latitude bin for both hemispheres GPM has a more bimodal distribution. For all latitudes GPM exhibits a strong peak near  $D_m = 1$  mm.

The right panel of Fig. 5 follows the same format but for derived  $N_w$ . The most striking aspect of these histograms is the strongly peaked distribution retrieved by GPM in all locations. In contrast, the disdrometers observe many cases with  $N_w$  values an order of magnitude greater or smaller than those of the GPM distributions. This would appear to have two leading, plausible explanations. First, OceanRAIN is expected to observe more variability in the number of drops because it is a point measurement integrated over one minute and precipitation characteristics can vary widely over multiple kilometers, whereas DPR has a 5 km footprint. Second, DSD retrieval from GPM is very much an under-constrained problem despite the unique capabilities of DPR. While the altitude mismatch between ground-based disdrometers and the GPM data at a few hundred meters altitude may cause some systematic differences, say due to some evaporation unseen by GPM, this does not explain the limited range of  $N_w$  values retrieved by GPM. The strongly peaked  $N_w$  distributions seem indicative of the significant influence of the a priori state on retrieval of  $N_w$ , in addition to the limited sensitivity to small number concentrations dictated by the instrument sensitivity of DPR.

## 4 Applicability of the modified gamma distribution

### 3.1 Overall behavior

Without applying any sorting methods or functional forms to the OceanRAIN data, it is worth viewing the data as a whole to see how closely the bulk-overall behavior resembles the distributions-MGD, as this is commonly used in the literature. Figure 3 shows a two-dimensional probability density function (PDF) of drop diameter normalized by  $D_m$  versus number concentration normalized by  $N_w$ . This is a view of bulk-drops' overall behavior often used to justify usage of the MGD-NG for precipitation (Bringi et al., 2003; Leinonen et al., 2012), as it permits visualization of in situ data points with the MGD-NG for various  $\mu$  values including the exponential DSD. Figure 3 indicates that much of the spectral power within OceanRAIN lies near the exponential ( $\mu=0$ ) line or near the lines with small-near-zero shape parameters. This is consistent with the enduring popularity of exponential DSDs and the  $\mu = 2$  assumption of GPM CombinedCORRA.

### 3.1 Comparison to GPM CORRA

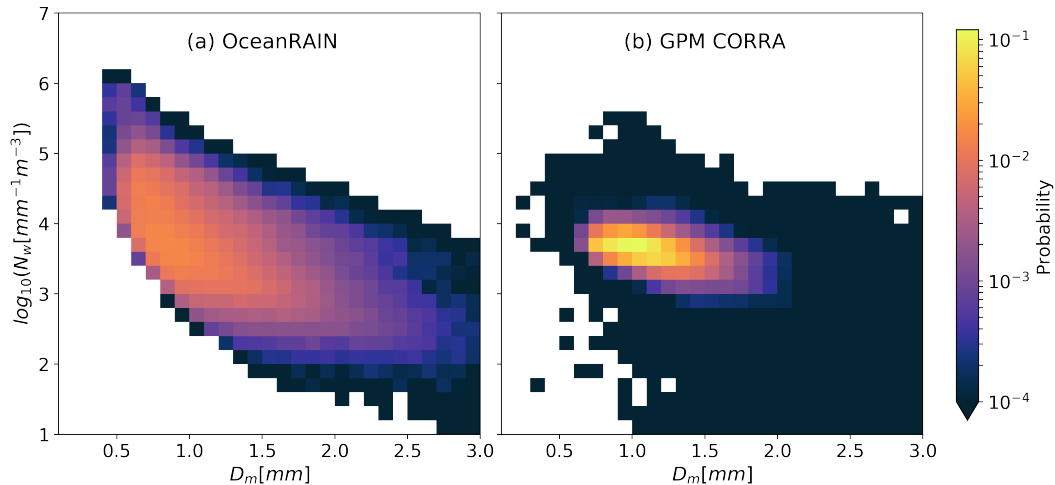


**Figure 4.** Probability density function of all raining histograms for OceanRAIN data points, visualized using (a) and GPM CORRA (b) for observations of the sealed-DSD,  $N(D)/N_w$ , against normalized intercept parameter ( $N_w$ ) and the diameter-normalized by mass-weighted mean diameter ( $D_m$ ). Various curves with prescribed  $\mu$  values are plotted for comparison. Areas in gray/white indicate no data.

To examine the applicability of the normalized gamma distribution to observed ocean DSDs, we can compare the observed PDF (Fig. 3) with the PDF generated after performing the 3-parameter MGD fit. This is shown in Fig. 11(a), with sample MGD curves given for extreme values of the shape parameter. The MGD-derived PDF overestimates the frequency of points near the exponential line and understandably displays less spread; blue areas indicate over-representation from the MGD fit, red areas indicate under-representation from the MGD fit. As with comparison between the PDF and MGD curves in Fig. 3, this shows an underestimation of small drops at high number concentrations through virtue of being constrained by the MGD fit.

To see if there is some regional dependence within the overall OceanRAIN PDF, Fig. 11(b) divides the data into observations from high-latitude (latitudes greater than  $50^\circ$ ) and tropical (latitudes less than  $20^\circ$ ) locations. It appears that whereas the MGD with a shape parameter ranging from  $\mu = 0$  to  $\mu = 3$  suffices for many tropical cases, high-latitude observations are not always well-represented by this formalism. For high-latitude oceanic rainfall, Figure 4 shows two-dimensional histograms of  $N_w$  versus  $D_m$  for both OceanRAIN and GPM CORRA. Both datasets exhibit an inverse relationship between  $N_w$  and increasing  $D_m$  and show maximum probabilities of occurrence in the same area, namely near  $D_m = 1\text{mm}$  and  $\log_{10}(N_w) = 3.8$ . The disdrometers show greater spread in both parameters, but especially in  $N_w$ . Whereas both data sets observe most occurrences of  $D_m$  between about 0.6 to 1.8 mm, the range of  $N_w$  observed by the disdrometers is easily twice as large, even in log space. This behavior is also seen in Fig. 11(b) demonstrates that small drops are underestimated and medium drops overestimated if using the MGD with 3 moments or fewer.

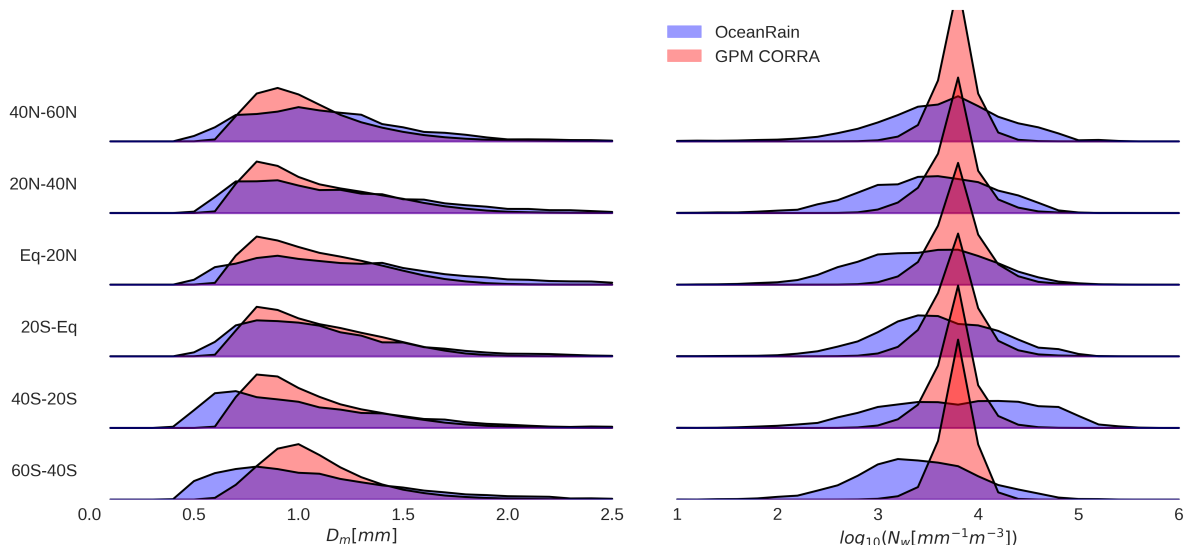


**Figure 5.** As in Fig. 3, but differences Normalized histograms of PDFs. The left panel  $D_m$  (left) shows the MGD-fitted PDF subtracted from the full OceanRAIN PDF shown in Fig. 3. The right panel and  $\log_{10}(N_w)$  (right) shows the difference of OceanRAIN PDFs from high-latitude for GPM CORRA and tropical oceanic locations OceanRAIN, viz separated by latitude.  $PDF_{>50^\circ} - PDF_{20^\circ N - 20^\circ S}$ , given as All histograms use a percent difference linear y-axis of height 20%. Areas in gray indicate no GPM data in one or both PDFs. The low and high  $\mu$  curves given approximately bound are from the PDF space for the MGD-fitted data 3B CMB monthly gridded product.

One concern raised by the results The left panel of Fig. 11 is whether the use of the MGD, and its limited representation of the full PDF of drop sizes, can cause biases in modeled or retrieved rain rates. To examine this is quite straightforward, in that a size-dependent terminal velocity (Atlas and Ulbrich, 1977) can be assigned for drops of each size bin, with the rain rate calculated as the integral product of the velocity distribution and the third moment of  $N(D)$ . This can then be compared between DSD representations. Using all raining OceanRAIN observations, use of the MGD fit was found to result in a small overestimation of rain rates, by  $0.06 \text{ mm h}^{-1}$  or 1.9%. Using the same definitions as above, this underestimation was slightly

less pronounced at high latitudes than for tropical locations, 1.5% versus 2.1%. This is due to underestimation of small drops by the MGD fit, as small drops have lower terminal velocities than larger drops, and with RWC being equal this can have a minor impact on resultant fluxes of precipitation. 5 shows histograms of derived  $D_m$  from the disdrometers compared with GPM CORRA, separated by latitude, with each latitude band 20 degrees wide. Given the limited sensitivity of DPR to small drops, it is unsurprising to note that OceanRAIN observes a wider distribution of  $D_m$  that is clearly different from GPM results for small drops. Another key feature of these histograms is that while the maxima in  $D_m$  distributions are relatively similar for the two data sets, OceanRAIN observes a less peaked distribution in most latitude bands. The disdrometers observe more small drops in all latitude bands, but this is especially pronounced in the Southern Ocean. For all latitudes GPM exhibits a peak near  $D_m = 1$  mm or just below.

Much of The right panel of Fig. 5 follows the same format but for derived  $N_w$ . The most striking aspect of these histograms is the strongly peaked distribution retrieved by GPM in all latitude bands. In contrast, the disdrometers observe many cases with  $N_w$  values an order of magnitude greater or smaller than those of the spread that exists in the full OceanRAIN PDF is due to the use of raw observational data that contain discontinuities between size bins and some degree of instrument error. It is clear, however, that much of GPM distributions. The peak  $N_w$  values from the disdrometers are similar to those of GPM CORRA in the spectral power in Fig. 3 is not captured by any one MGD curve. While the exponential line and  $\mu = 3$  curves do a reasonable job at matching the PDF for larger drop sizes, the  $\mu = 2$  curve performs much better for smaller diameters. This suggests that a 4-parameter “generalized gamma” fit might be optimal for ocean DSDs, a finding echoed in another recent study of disdrometer data (Thurai and Bringi, 2018). Use of the 3-parameter MGD can lead to some systematic biases in drop size representation as seen in Fig. 11(a). These biases can be regionally dependent, as shown by the higher number concentrations of small drops seen in high latitudes relative to the tropics, as seen in Fig. 11(b). northernmost latitude band, but are significantly wider and flatter in every latitude band shown.

### 3.2 GMM states

#### 4 GMM-derived states

As shown in Fig. 3, the MGD-NG with a low  $\mu$  value does a reasonable job at capturing the main power lies near the highest probability densities of the observed PDF. However, a great deal of spread exists that is not captured by any one curve. With this in mind, GMM was employed to investigate if a finite number of DSD shapes without a predefined functional form could better capture this variability.

To provide a visualization of how the GMM states attempt to fit the observed DSD from the disdrometer, and how these states compare with various MGD forms, Fig. 6 contains randomly sampled data points from OceanRAIN. These four data points have quite different rain rates and RWCs. The GMM curves shown are from iterations with  $N_{GMM}$  of 6 and 14, two of the panels given in the subsequent figure; these are the states with the highest posterior probability from GMM, indicating the best match to the observed distribution. No fitting was performed (other than scaling by the correct observed RWC), just the most similar GMM curve was chosen, judged by the highest posterior probability. Also provided for reference are MGD

curves with 1-, 2-, and 3-moment 3-parameter fits. The MGD 1- and 2-moment 1-parameter MGD fits represent RWC-only and RWC and  $D_m$  fits, respectively, with a nominal shape parameter assumed. fits, with  $\mu = 3$  and  $D_m = 1.18\text{mm}$  prescribed. For the 2-parameter MGD fit,  $D_m$  is calculated via Eq. 2 and  $\mu = 3$  is prescribed. All the curves in Fig. 6 have the correct conserve total RWC as measured by the disdrometer.

Figure 6 shows a variety of observed DSDs from different locations and SST regimes. In these plots the size bins below 0.4 mm are greyed out to signify the disdrometers' insensitivity to these drop sizes. The discontinuities between size bins are noticeable in some panels at larger drop diameters, especially the fourth panel. The second panel is the most exponential distribution of the four shown, while the first panel shows a DSD that fits well with the MGD with  $\mu = 3$  and a small  $D_m$ . The third panel shows a heavy tropical rainfall case with bimodal characteristics, as a high concentration of drops smaller than  $D = 0.8\text{mm}$  is observed but significant concentrations of drops larger than  $D = 2\text{mm}$  also exist. In this particular case the GMM-derived curves appear to provide the best fit but are still imperfect.

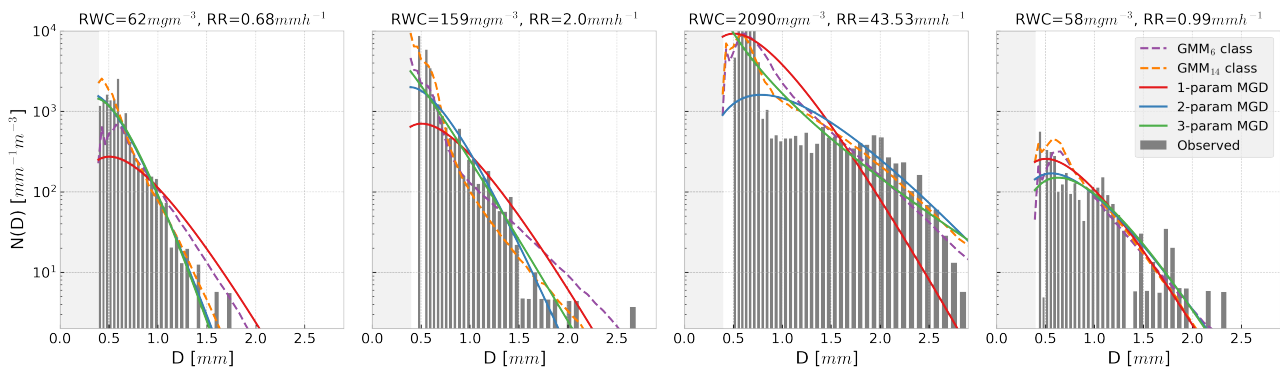


**Figure 6.** Each panel gives an OceanRAIN observed DSD, with concentrations shown seen in the solid bars. Various fitted curves with identical RWCs are also given, including GMM-derived DSDs for  $N_{GMM}$  of 6 and 14, and 3 MGD curves. For the 1-moment 1-parameter MGD and GMM curves only RWC is provided, and for the 1- and 2-moment 2-parameter MGD curves  $\mu = 3$ . The 2-moment 2-parameter MGD has the correct calculated  $D_m$  while the 3-moment 3-parameter MGD (i.e. NG) also has the fitted  $\mu$ . Each data point is identified by its RWC and rain rate. The light gray shaded region indicates an area of no OceanRAIN sensitivity.

In contrast to the example plots of Fig. 6, Fig. 7 shows the mean GMM curves that arise from running GMM with a few different  $N_{GMM}$  values. Again, this is from running GMM on the raw disdrometer full disdrometer size bin data, with only the number of classes set a priori. For comparison, reference lines of MGD-NG distributions with sample  $\mu$  and  $D_m$  values are also given. Note that for each panel in Fig. 7, a majority of the GMM-derived DSDs feature more small drops than given by even the exponential ( $\mu = 0$ ) line. In the simplest case with only two classes possible (first panel of Fig. 7), the DSD shape that best captures the majority of the OceanRAIN data set's variability (at least in terms of frequency of occurrence) is a shape that is more sloped than the exponential DSD, with many small drops and very few large drops. This particular shape is common to all the GMM realizations, with even more steeply sloped steeper curves found as GMM states are added. Indeed, the distributions

produced by GMM seldom resemble a pure exponential DSD. It is an indication that a second shape parameter may be useful for describing oceanic DSDs, in line with the generalized gamma approach argued for by Thurai and Bringi (2018).

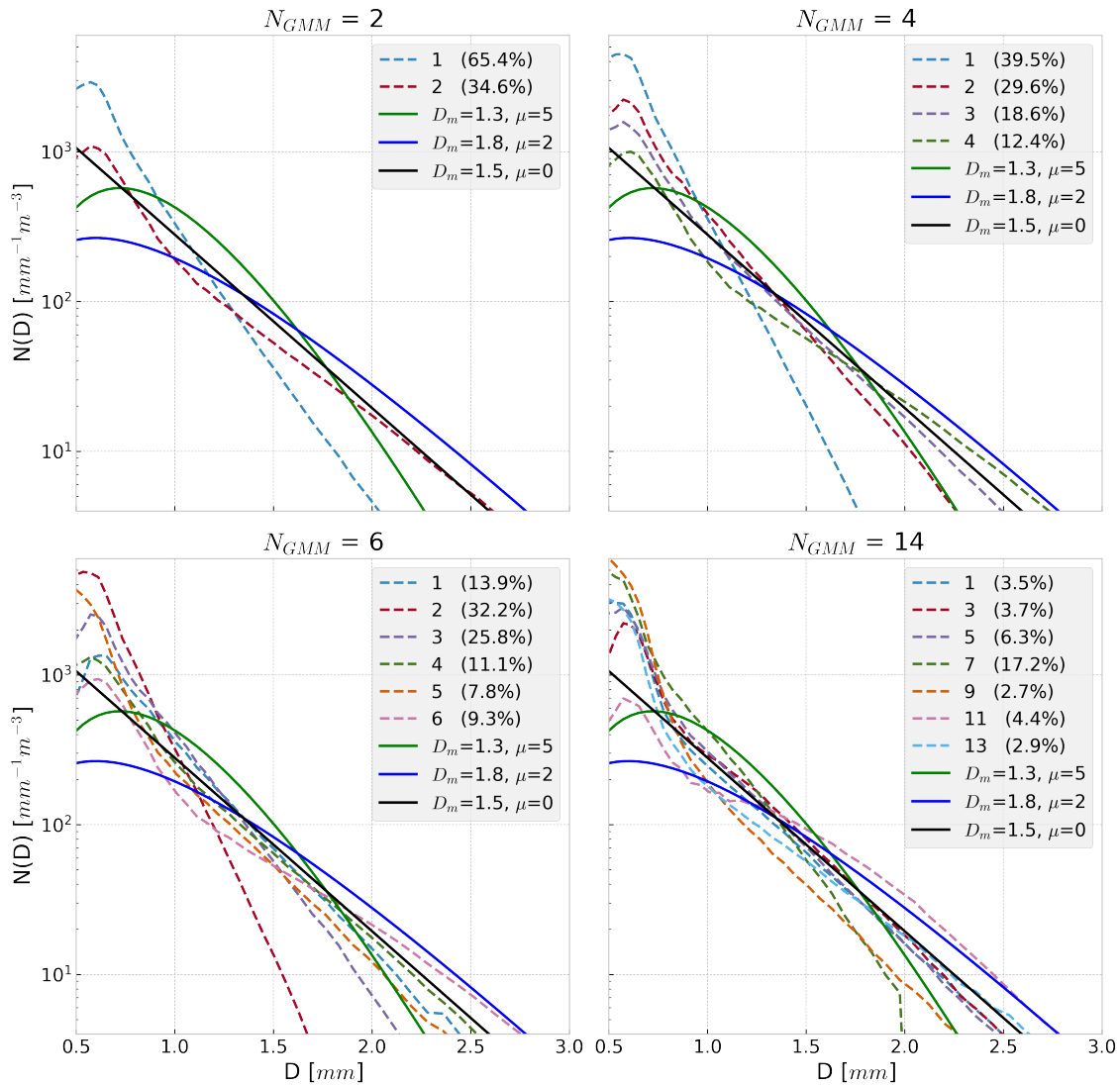


**Figure 7.** Panels show resultant DSDs for different GMM realizations (dashed lines) ranging from  $N_{GMM}$  of 2 to 14. The last panel shows only odd numbered GMM states to reduce clutter. Each panel has an identical set of MGD-NG curves with different  $\mu$  and  $D_m$  values (solid lines) for the sake of comparison. All curves shown have the same water content equal RWC. The frequency of occurrence for each GMM shape is given in the legend as a percentage.

It is noteworthy that most of the GMM states shown in Fig. 7 are not similar to the given MGD-NG curves across the full range of drop diameters. So while some of the GMM states are quite like a particular MGD-NG curve over part of the domain,

it is rare to ~~have observe~~ DSD shapes from individual ~~observations-minutes~~ that resemble a ~~3-moment-MGD-3-parameter~~ ~~MGD (i.e. NG)~~ across the whole size domain. In many cases the GMM method prefers states with more steeply sloped DSDs and more small drops than the sample ~~MGD-NG~~ curves given. In fact, it takes higher values of  $N_{GMM}$  (such as in Fig. 7 with  $N_{GMM}=14$ ) before strongly peaked DSD shapes reminiscent of ~~MGD-NG~~ with a large  $\mu$  value emerge. In other words,

10 DSDs ~~with few small drops, featuring~~ a strong peak ~~of drops around near~~  $D_m$ , and for which an exponential is a ~~very~~ poor approximation, are ~~not very common~~ ~~infrequent~~. This can also be seen in Fig. 3, as ~~scant spectral power is seen near the PDF is~~ ~~relatively weak in~~ the bottom left of that plot.

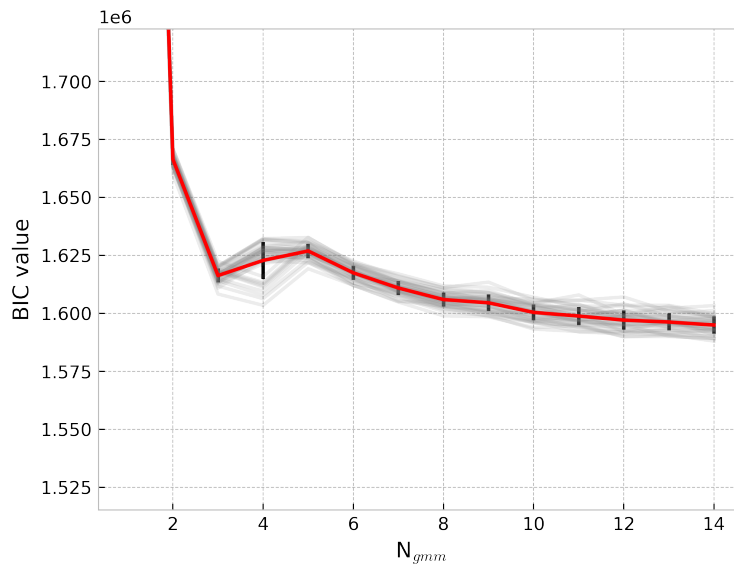


**Figure 8.** Bayesian Information Criterion (BIC) for different  $N_{GMM}$  choices applied to OceanRAIN. The mean BIC is shown in red with the standard deviation in black. Gray lines indicate GMM tests with limited samples, each a randomly chosen subset making up a third of the total data set.

The GMM framework as applied to the DSD problem seems to offer the promise of finding a finite number of distinct shapes with which global DSD variability can be described, a la Dolan et al. (2018), ~~with the benefit of not without~~ constraining the

15 type of shapes found. To investigate this, GMM was used in many iterations for randomly sampled subsets of the data to assess if an optimal number of states exist that describe the global shape variability. In this experiment  $N_{GMM}$  was varied from 2 to ~~12-14~~. The Bayesian Information Criterion (Eq. 6) gauges whether ~~adding further states better describes the data or not~~ ~~addition~~ ~~of further states provides a better description of the data~~, shown in Fig. 8. BIC plateaus and continues a slight decrease for GMM states beyond about  $N_{GMM} = 8$ , indicating that there is no singular set of GMM-derived DSD shapes that outperforms the others. Instead, oceanic DSD shape variability proves to be a true continuum that is not easily decomposed into a linear combination of a finite set of curves.

5 A corollary of the finding that a singular, optimal set of GMM-derived curves does not exist is that the observed DSD shapes do not display ~~particularly~~ predictable regional patterns. The shapes observed are not ~~especially distinct when decoupled from RWC~~ distinct when normalized by RWC, whether considering the DSDs regionally or ~~say~~ across SST regimes. The GMM-derived shapes are not ~~particularly~~ tied to one region or another, a finding that echoes Fig. 2. This is in contrast to some studies' success in pulling regional attributes out of large data sets via GMM without including location information, as was done here  
10 (Jones et al., 2019). The only area of OceanRAIN sampling that ~~is particularly appears as~~ distinct in the distribution of GMM states is from observations in stratocumulus regions, ~~where~~ which are dominated by the GMM states ~~characterized by with~~ steeply sloped DSD curves ~~with and~~ a large number of small drops ~~are dominant~~. Otherwise, the GMM states are not strongly tied to particular sampling regions. This tendency changes if DSD is not ~~decoupled from~~ normalized by RWC, as RWC regimes are more tied to regional meteorology. But with respect to the retrieval problem, where it is convenient to separate the DSD  
15 shape from RWC as in Eq. 3, the GMM approach does not provide a magic bullet.

## 5 Radiative transfer impacts

An overlooked aspect of assuming a DSD a priori, or even just assuming the general shape of the DSD a priori, is that this will introduce forward model errors in retrievals and data assimilation. These errors can be strongly correlated across nearby frequencies and can thus cause systematic biases in variational systems (e.g. 1DVAR, 3DVAR) if not taken into account. An  
20 example of including this type of forward model error into a variational rainfall retrieval for GPM was presented by Duncan et al. (2018). Instead, the focus in this section is investigating the extent of forward model response inherent to variations in natural drop populations, without fitting a functional form to the observed drop counts. Because ~~water content~~ RWC or rain rate is usually the sought parameter from remote sensing retrievals, the results are separated along those lines.

~~The~~ Forward model simulations of the radiative transfer were performed using the Atmospheric Radiative Transfer Simulator (ARTS) version 2.3 (Eriksson et al., 2011; Buehler et al., 2018) ~~was used to perform forward model simulations~~. The ARTS  
25 model can handle custom particle size distributions ~~and habits as~~ (such as observational size bin data) as well as prescribed DSDs such as the MGD. Thus with the full ~~raw~~ size bin data from OceanRAIN it is possible to simulate the interaction of radiation with drop populations without making any simplifications involving the drops' functional form. To approximate the impact on a sensor such as GMI on GPM, simulations were run using the GMI geometry and three GMI frequencies: 18.7, 36.64, and  
30 89.0 GHz. Because the surface-based disdrometer data inherently lack vertical information, hydrometeor and humidity profiles need to be assumed. To avoid complications from inclusion of any ice scattering species, the setup is for warm rain: a 1 km rain layer defined by the RWC and DSD observed, with a 1 km liquid cloud layer of ~~200 g m<sup>-2</sup> above~~ 0.2 kg m<sup>-2</sup> above, characteristic of a raining warm cloud (Lebsock et al., 2008). Here we differentiate between cloud water and rainwater due to their different radiative characteristics, with the total liquid water path being the sum of the two. The surface properties and humidity profile are typical of a tropical scene, with the surface emissivity calculated using the Tool to Estimate Sea-Surface Emissivity from Microwaves to sub-Millimeter waves (TESSEM2), which is embedded in ARTS (Prigent et al., 2017). DSD properties are constant within the rain layer and the cloud layer is also homogeneous. Cloud droplets are monodisperse with

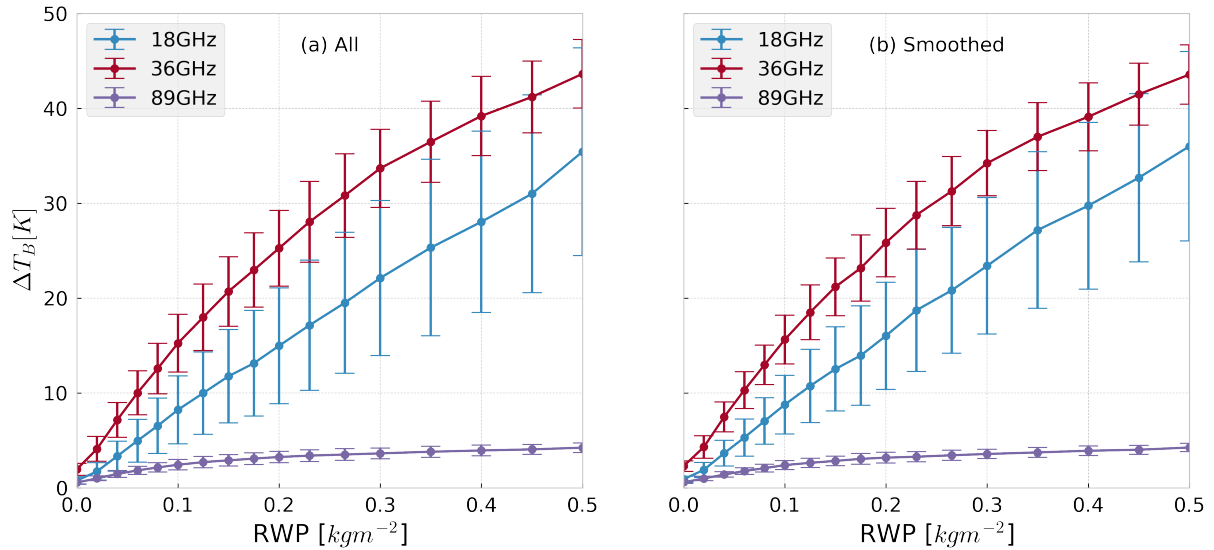


**Figure 9.** Simulated brightness temperatures ( $T_B$ ) through a modeled atmosphere for warm rain, with a liquid cloud layer of  $200 \text{ g m}^{-2}$   $0.2 \text{ kg m}^{-2}$  from 1 to 2 km altitude and rain in the lowest kilometer. The **water content RWC** in the rain layer and the DSD are directly from disdrometer observations and constant in the rain layer. Given are the means (dots) and standard deviations ( $\pm 1\sigma$ , shown as bars) of  $\Delta T_B$  per rain water path (RWP) bin, where the difference in  $T_B$  is defined relative to  $RWP = 0$ . The left panel (a) uses all OceanRAIN observations, the right panel (b) shows results when averaging over consecutive 6 minute observation windows to approximate a satellite footprint.

5 diameter  $15 \mu\text{m}$ , whereas the rain drops are about two orders of magnitude larger in diameter, hence their differing scattering properties. Simulation code is available (Duncan, 2019).

Figure 9(a) shows the results of the GMI simulations using native disdrometer data, with rain water path (RWP) simply RWC vertically integrated over the 1 km rain layer, given in  $\text{kg m}^{-1}$ . The change in radiance top of atmosphere radiance in Kelvin,  $\Delta T_B$ , is defined relative to the non-raining case of  $RWP = 0$  and for unpolarized radiation. With no mixed phase or ice phase hydrometeors in the atmospheric column, the three GMI channels chosen all exhibit a net increase in  $T_B$ . The 89 GHz shows little impact from sensitivity to either DSD variability or an increase in RWP, as; its signal is mainly from cloud water emission, as the scattering and the scattering signal from rain largely cancels out its emission signal from rain. In contrast, the lower frequency channels show large increases in  $T_B$  with RWP as emission dominates and the cloud is more transparent, with the wide range of scattering response showing the strong dependence on drop size. The 18 GHz  $T_B$  especially shows large variability for a given RWP, with the standard deviation of the  $T_B$  response usually about half of the net response mean value. This is a significant error source for warm rain estimation, as the difference between a RWP of 0.2 and 0.3  $\text{kg m}^{-2}$  would be difficult to distinguish using these frequencies alone due to the overlapping forward model error bounds.

To address the point-to-area issue of comparing OceanRAIN observations integrated every minute with those of a spaceborne passive microwave or radar footprint, which is 5 km in the best case, Fig. 9(b) shows a sample result if the disdrometer data

5 are averaged in time. Averaging in time is performed because it approximates a spatial average, absent other observing points. Specifically, a nominal 6-16 minute window was used to average consecutive raining disdrometer measurements. ~~Non-raining points~~, in that a ship at 10 kn would take about 16 minutes to traverse 5 km. Observations with zero rain rates were not included ~~or added~~ if the OceanRAIN points were discontinuous in time. Fig. 9(b) shows that the results are quite similar to the native disdrometer data used in panel (a), ~~and thus the~~ with standard deviations slightly smaller for lower  $RWP$  values. The maximum forward model errors observed by a sensor such as GMI ~~should may~~ not be markedly different ~~than those presented with the time averaging performed, however most GMI channel footprints are larger than that of DPR.~~

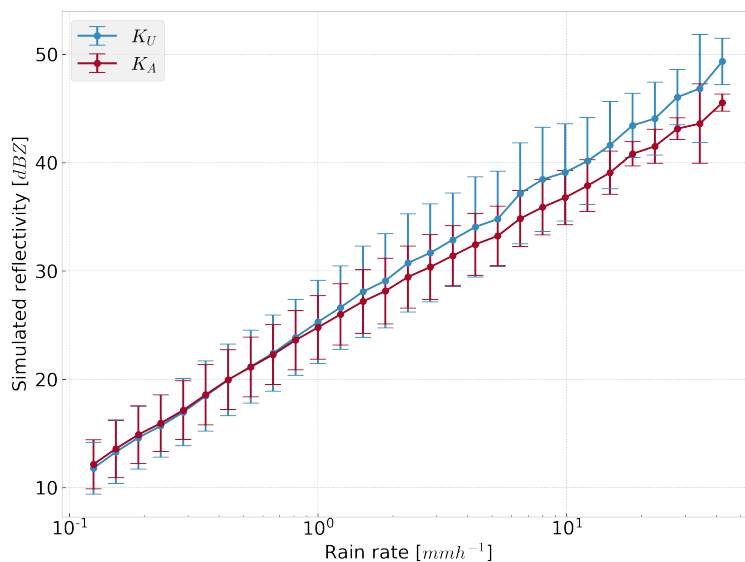


**Figure 10.** Simulated radar reflectivities at the two DPR frequencies,  $K_U$  and  $K_A$  bands, shown as means (dots) and standard deviations ( $\pm 1\sigma$ , shown as bars) binned by rain rate. The rain rate and the DSD are directly from OceanRAIN observations.

Without needing to assume a model atmosphere, the variability of radar reflectivities can be simulated with the measured volume of drops alone and the T-matrix method (Klepp et al., 2018). Figure 10 gives the simulated radar reflectivity response over a range of rain rates using the OceanRAIN observations. As with the passive sensor simulations, this demonstrates that DSD variability can cause significant differences in the radiative properties of a volume of drops even for equivalent rain rates or ~~water contents~~  $RWC$ s. As with Fig. 9, the range of scattering response is larger for the lower frequency channels, with  $K_U$  showing greater variability in modeled reflectivity, as the specifics of the DSD determine whether the drops' scattering is wholly in the Rayleigh regime or partly in the Mie regime. The  $K_A$  band is less ~~effected~~ ~~affected~~ by DSD variations in both the passive and active simulations while scaling mostly linearly with increasing  $RWC$  or rain rate.

## 6 Discussion

### 6.1 Comparison with GPM

The discrepancies between OceanRAIN and GPM histograms of retrieved  $D_m$  and  $N_w$  (Figs. 4 and 5) deserve some discussion. The distributions of  $D_m$  and  $N_w$  from disdrometer measurements are wider than those from GPM CORRA retrievals in most latitude bands, significantly so for  $N_w$ . GPM has limited sensitivity to small drops and lower number concentrations due to the minimum detectable signal from DPR, which may explain the small drops underestimated relative to the disdrometer measurements, especially in the Southern Ocean.

The highly peaked GPM distributions of  $N_w$ , in stark contrast to OceanRAIN's much flatter  $N_w$  distributions at all latitudes, would appear to have two leading, plausible explanations. First, OceanRAIN is expected to observe more variability in the number of drops because it is a point measurement integrated over one minute and precipitation characteristics can vary widely over multiple kilometers, whereas DPR has a 5 km footprint. Second, DSD retrieval from GPM is an under-constrained problem (more unknowns than information) despite the unique capabilities of DPR. While the altitude mismatch between surface-based disdrometers and the GPM data at a few hundred meters altitude may cause some systematic differences, say due to evaporation unseen by GPM, this does not explain the limited range of  $N_w$  values retrieved by GPM. The strongly peaked  $N_w$  distributions seem indicative of the significant influence of the a priori state on retrieval of  $N_w$ , in addition to the limited sensitivity to small number concentrations dictated by the instrument sensitivity of DPR.

### 6.2 Applicability of the modified gamma distribution

To examine the applicability of the MGD to observed ocean DSDs, we can compare the observed PDF (Fig. 3 and Fig. 11(a)) with the PDF of the same data but constrained by the NG fit (Fig. 11(c)). This is shown in Fig. 11(e), with sample NG curves given for extreme values of the shape parameter. The NG-derived PDF overestimates the frequency of points near the exponential line and displays less spread; blue areas indicate over-representation from the NG fit, red areas indicate under-representation from the NG fit. As with comparison between the PDF and NG curves in Fig. 3, this shows an underestimation of small drops at high number concentrations through virtue of being constrained by the NG fit.

To see if there is some latitudinal dependence within the overall OceanRAIN PDF, Fig. 11(b,d) divides the data into observations from high latitude (latitudes greater than  $50^\circ$ ) and tropical (latitudes less than  $20^\circ$ ) locations. It appears that whereas the NG with a shape parameter ranging roughly between  $\mu = 0$  to  $\mu = 3$  suffices for many tropical cases, high latitude observations are not always well represented by the 3-parameter MGD. For high latitude oceanic rainfall, Fig. 11(f) demonstrates that small drops are underestimated and medium drops overestimated if using the 3-parameter MGD.

One concern raised by the results of Fig. 11 is whether the use of the 3-parameter MGD, and its limited representation of the full PDF of drop sizes, can cause biases in modeled or retrieved rain rates. To examine this is quite straightforward, in that a size-dependent terminal velocity (Atlas and Ulbrich, 1977) can be assigned for drops of each size bin, with the rain rate calculated as the integral product of the velocity distribution and the third moment of  $N(D)$ . The calculated rain rate can then be compared between DSD representations. Using all OceanRAIN observations shown in Fig. 1 we calculated rain rates

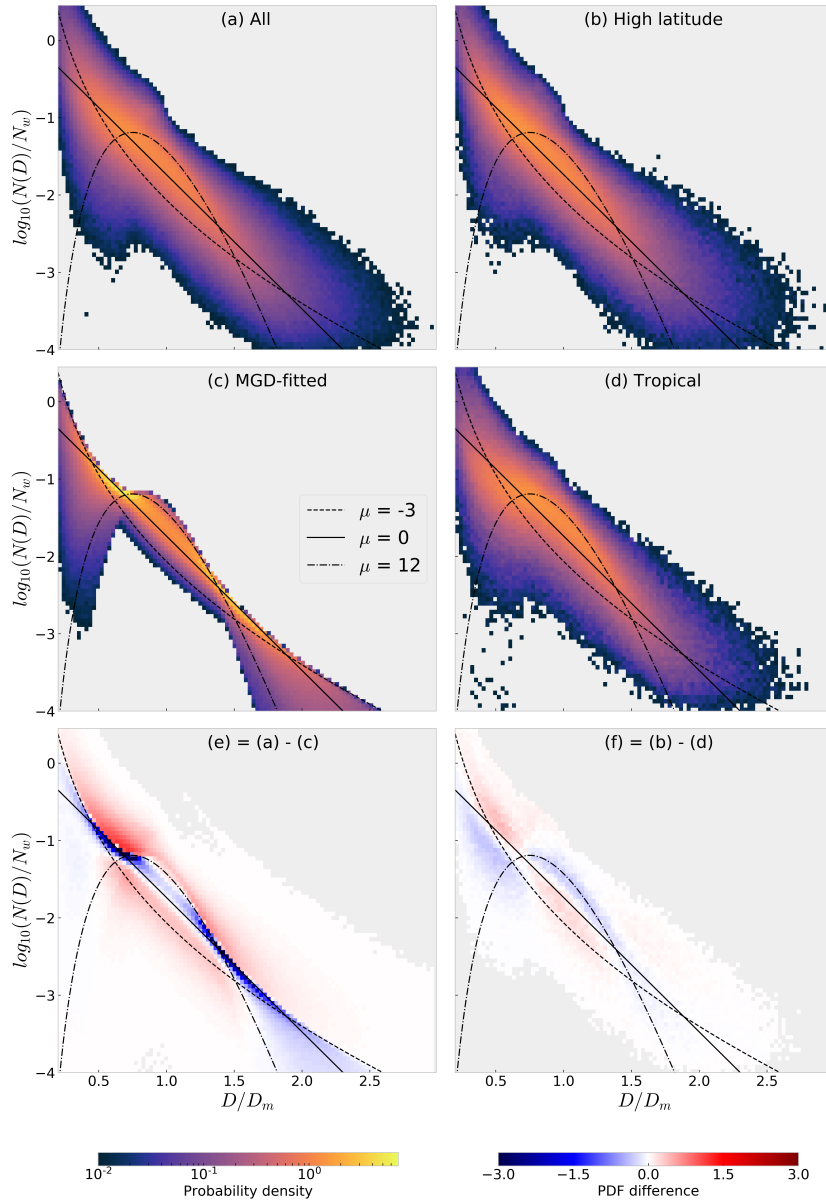


**Figure 11.** Panel (a) duplicates the result in Fig. 3. Panel (c) shows the data from (a) but after fitted to the NG distribution. The bottom left (e) shows the NG-fitted PDF subtracted from the full PDF. The right panels show OceanRAIN PDFs from high latitude (b) and tropical (d) latitudes, viz.  $PDF_{>50^\circ}$  and  $PDF_{20^\circ N-20^\circ S}$ , with their difference given in (f). Areas in gray indicate no data. The low and high  $\mu$  curves given approximately bound the PDF space for the fitted data. Panels (a)-(d) share the same color scale and panels (e) and (f) also share the same anomaly color scale.

manually using the size bin data and assuming terminal velocities for all drops, allowing comparison of the rain rates that arise from the PDFs shown in Fig. 11 panels (a) and (c). The distributions resultant from the NG fit was found to result in a small mean overestimation of rain rates, by  $0.06 \text{ mm h}^{-1}$  or 1.9%. Using the same definitions as above, this underestimation was slightly less pronounced at high latitudes than for tropical latitudes, 1.5% versus 2.1%. This is due to underestimation of small drops by the NG fit, as small drops have lower terminal velocities than larger drops, and with RWC being equal this can have a minor impact on resultant fluxes of precipitation.

Much of the spread that exists in the full OceanRAIN PDF is due to the use of unsmoothed observational data that contain discontinuities between size bins and some degree of instrument error. It is clear, however, that much of the spectral power in Fig. 3 is not captured by any one NG curve. While the exponential line and  $\mu = 3$  curves do a reasonable job at matching the PDF for larger drop sizes, the  $\mu = -2$  curve performs much better for smaller diameters. This suggests that a 4-parameter “generalized gamma” fit might be optimal for oceanic DSDs, a finding echoed in another recent study of disdrometer data (Thurai and Bringi, 2018). Use of the 3-parameter MGD can lead to some systematic biases in drop size representation as seen in Fig. 11(e). These biases can be regionally dependent, as shown by the higher number concentrations of small drops seen in high latitudes relative to the tropics, as seen in Fig. 11(f), and consistent with findings from Dolan et al. (2018).

## 7 Summary and conclusions

This study has investigated the variability of raindrop size distributions over the global oceans in a variety of contexts relevant to retrievals and atmospheric modeling. Methods to attach a functional form to raindrop populations vary, but have largely been predicated on limited land-based observations in the past. The OceanRAIN observation network of disdrometers provides an opportunity to move towards better understanding of global raindrop populations, with ramifications in aid of satellite retrievals and model parameterizations, which are necessarily global in scope.

The disdrometer data were shown to have limited dependence on latitude or SST (Fig. 2) when quantified using parameters of the normalized gamma distribution (Eq. 3). The mean and median of  $D_m$  tend to vary within 0.1 mm across all regions/latitudes, with  $\pm\sigma$  of about 0.2 mm. Most observations of  $\log_{10}(N_w)$  fall within 3.0 to 4.3 (Fig. 4), with a weak correlation observed exhibited between  $N_w$  and SST (Fig. 2). These parameters from OceanRAIN were also compared to the leading estimates from a satellite platform (Fig. 5); comparisons with GPM matched relatively well for distributions of  $D_m$  but less so for  $N_w$ . Both parameters appear to be too peaked from the GPM retrieval, likely a result of strong influence from that retrieval’s a priori state as  $D_m = 1.0$  and  $\log_{10}(N_w) = 4.0$  was commonly seen DSDs with approximately  $D_m = 1.0 \text{ mm}$  and  $\log_{10}(N_w) = 3.9$  were frequent. The data sets observe-exhibit similar spreads in the distributions of  $D_m$ , but the disdrometers observe-show significantly more variability in  $N_w$  than seen by GPM; the middle 90% of GPM  $N_w$  retrievals fall within one order of magnitude, whereas the middle 90% of disdrometer observations span 2.2-over 2 orders of magnitude. It is-was speculated that the GPM retrievals may be over-constrained, although it was expected that the point measurements of the disdrometer would display greater variability than those from satellite sources due to spatial and temporal considerations alone.

Usage of the normalized gamma ~~function to encapsulate the~~ distribution to describe all observed DSD behavior was questioned (Section 6.2), as it appears more applicable in the Tropics than for higher latitude populations. High latitude cases exhibit larger concentrations of small drops that are outside the state space specified by the 3-parameter MGD (Fig. 11). ~~Its use~~ The 3-parameter MGD can cause systematic biases in rain rate estimation relative to using the observed size bin data, quantified to be ~~in the mean~~ a -2% error in the mean relative to total accumulation calculated ~~with the raw disdrometer size data from the disdrometers~~. This is a relatively small error for total accumulation because the ~~smallest~~ drops that are most misrepresented by the normalized gamma formalism account for relatively little of the total mass flux, ~~however;~~ however, for about 3% of cases this is an error of  $-0.5 \text{ mm h}^{-1}$  or more, and can thus be significant. For many applications, an exponential DSD ~~would may~~ be simpler and more appropriate than a MGD-NG distribution for oceanic rainfall (Fig. 3), but of course does not encapsulate the range of variability that exists, which may be better represented by a generalized gamma approach with four parameters (Thurai and Bringi, 2018).

Radiative properties of raindrop populations can vary rapidly for low frequency microwaves, manifest in Fig. 9 as ~~uncertainty makes up approximately half the~~ the standard deviation magnitude is approximately half of the net radiative signal at 18 GHz but is much less at higher frequencies such as 89 GHz. This is because the presence of a few larger drops can cause non-negligible Mie scattering that impacts the otherwise emission-dominated radiative signal and Rayleigh scattering from smaller drops, an effect that diminishes as frequency increases. Fig. 10 also showed this effect, with lower frequencies exhibiting greater ~~uncertainty variability~~ for a given RWC or rain rate due to observed DSD variability. Whereas the radiative ~~uncertainty variability~~ is similar for light rain rates, modeled variability can be 2-3 times greater at  $K_U$  rather than  $K_A$  band, ~~true for~~ This observed  $T_B$  variability caused by DSD variability is seen in both passive and active simulations. These ranges of forward model variability however represent a worst case scenario for satellite retrievals or data assimilation, as any skill in assuming or retrieving the DSD would shrink these ranges. This passive forward model variability can even be viewed favorably, as it demonstrates sensitivity to the DSD at low microwave frequencies that may aid DSD retrievals. Simulations comparing forward model errors caused by using a GMM-derived or MGD state compared to the true DSD state showed that a high  $N_{GMM}$  value was needed for the GMM states to outperform the ~~3-moment 3-parameter~~ MGD for forward model errors (not shown). This is in line with Fig. 8, but also indicative that it is hard for a single-moment scheme such as GMM to compete without having a large number of possible states.

This exploration of DSD shape “distinctiveness” was motivated by the remote sensing and modeling communities’ need for simple but accurate parameterizations of rainwater’s size distribution. For instance, if a region or ~~rainfall meteorological~~ regime tends to exhibit one or two DSD shapes, this simplifies a multidimensional problem considerably. The results, however, demonstrate that simple separation of DSD shapes by latitude and SST, or by other variables such as dewpoint temperature and RWC (not shown), does not significantly simplify the DSD problem. The limited spatiotemporal sampling of OceanRAIN meant that further subdivision of regional data for seasonal shifts in DSD was not possible. The conclusion is then that global oceanic DSD variability, though more uniform than over land surfaces, is complex and not easily reduced to a single moment parameterization or a small set of possible shapes.

*Code availability.* The code used for analysis is all available in the form of Jupyter notebooks via a Zenodo archive, found in the references.

*Author contributions.* DD and PE conceived and designed the study, inspired by discussions with and the work of CK and DJ. DD performed the analysis with aid from SP. DD wrote the manuscript and all authors contributed to its final form.

5 *Competing interests.* The authors declare that they have no conflict of interest.

*Acknowledgements.* This study was funded with support from the Swedish National Space Agency, for which DD, PE, and SP are grateful. DJ is supported by a grant from the Natural Environment Research Council (grant NE/N018028/1). The North Atlantic Climate System Integrated Study (ACSIS).

## References

- 10 Atlas, D. and Ulbrich, C. W.: Path- and Area-Integrated Rainfall Measurement by Microwave Attenuation in the 1–3 cm Band, *J. Appl. Meteorol.*, 16, 1322–1331, [https://doi.org/10.1175/1520-0450\(1977\)016<1322:PAAIRM>2.0.CO;2](https://doi.org/10.1175/1520-0450(1977)016<1322:PAAIRM>2.0.CO;2), 1977.
- Berg, W., L'Ecuyer, T., and Kummerow, C.: Rainfall climate regimes: The relationship of regional TRMM rainfall biases to the environment, *J. Appl. Meteorol. and Climatol.*, 45, 434–454, <https://doi.org/10.1175/JAM2331.1>, 2006.
- Bringi, V. N., Chandrasekar, V., Hubbert, J., Gorgucci, E., Randeu, W. L., and Schoenhuber, M.: Raindrop size distribution in different climatic regimes from disdrometer and dual-polarized radar analysis, *J. Atmos. Sci.*, 60, 354–365, [https://doi.org/10.1175/1520-0469\(2003\)060<0354:RSDIDC>2.0.CO;2](https://doi.org/10.1175/1520-0469(2003)060<0354:RSDIDC>2.0.CO;2), 2003.
- Buehler, S. A., Mendrok, J., Eriksson, P., Perrin, A., Larsson, R., and Lemke, O.: ARTS, the Atmospheric Radiative Transfer Simulator – version 2.2, the planetary toolbox edition, *Geosci. Model Dev.*, 11, 1537–1556, <https://doi.org/10.5194/gmd-11-1537-2018>, 2018.
- Bumke, K. and Seltmann, J.: Analysis of measured drop size spectra over land and sea, *ISRN Meteorol.*, 2012, <https://doi.org/10.5402/2012/296575>, 2011.
- 20 Burdanowitz, J., Klepp, C., Bakan, S., and Buehler, S. A.: Towards an along-track validation of HOAPS precipitation using OceanRAIN optical disdrometer data over the Atlantic Ocean, *Quart. J. Roy. Meteor. Soc.*, 144, 235–254, <https://doi.org/10.1002/qj.3248>, <https://rmets.onlinelibrary.wiley.com/doi/abs/10.1002/qj.3248>, 2018.
- Dolan, B., Fuchs, B., Rutledge, S. A., Barnes, E. A., and Thompson, E. J.: Primary Modes of Global Drop Size Distributions, *J. Atmos. Sci.*, 25 75, 1453–1476, <https://doi.org/10.1175/JAS-D-17-0242.1>, 2018.
- Duncan, D. I.: Supporting code for ACP submission on DSD distinctiveness, <https://doi.org/10.5281/zenodo.2653512>, 2019.
- Duncan, D. I., Kummerow, C. D., Dolan, B., and Petković, V.: Towards variational retrieval of warm rain from passive microwave observations, *Atmos. Meas. Tech.*, 11, 4389–4411, <https://doi.org/10.5194/amt-11-4389-2018>, <https://www.atmos-meas-tech.net/11/4389/2018/>, 2018.
- 30 Eriksson, P., Buehler, S., Davis, C., Emde, C., and Lemke, O.: ARTS, the Atmospheric Radiative Transfer Simulator, version 2, *J. Quant. Spectrosc. Radiat. Transfer*, 112, 1551–1558, <https://doi.org/10.1016/j.jqsrt.2011.03.001>, 2011.
- Greco, M., Olson, W. S., Munchak, S. J., Ringerud, S., Liao, L., Haddad, Z., Kelley, B. L., and McLaughlin, S. F.: The GPM Combined Algorithm, *J. Atmos. Oceanic Technol.*, 33, 2225–2245, <https://doi.org/10.1175/JTECH-D-16-0019.1>, 2016.
- Grossklaus, M., Uhlig, K., and Hasse, L.: An optical disdrometer for use in high wind speeds, *J. Atmos. Oceanic Technol.*, 15, 1051–1059, [https://doi.org/10.1175/1520-0426\(1998\)015<1051:AODFUI>2.0.CO;2](https://doi.org/10.1175/1520-0426(1998)015<1051:AODFUI>2.0.CO;2), 1998.
- 35 Hou, A. Y., Kakar, R. K., Neeck, S., Azarbarzin, A. A., Kummerow, C. D., Kojima, M., Oki, R., Nakamura, K., and Iguchi, T.: The Global Precipitation Measurement Mission, *Bull. Amer. Meteor. Soc.*, 95, 701–722, <https://doi.org/10.1175/BAMS-D-13-00164.1>, 2014.
- Illingworth, A. J. and Blackman, T. M.: The Need to Represent Raindrop Size Spectra as Normalized Gamma Distributions for the Interpretation of Polarization Radar Observations, *J. Appl. Meteorol.*, 41, 286–297, [https://doi.org/10.1175/1520-0450\(2002\)041<0286:TNTRRS>2.0.CO;2](https://doi.org/10.1175/1520-0450(2002)041<0286:TNTRRS>2.0.CO;2), 2002.
- Jones, D. C., Holt, H. J., Meijers, A. J. S., and Shuckburgh, E.: Unsupervised clustering of Southern Ocean Argo float temperature profiles, *J. Geophys. Res. Oceans*, 124, 390–402, <https://doi.org/10.1029/2018JC014629>, 2019.
- Klepp, C.: The oceanic shipboard precipitation measurement network for surface validation — OceanRAIN, *Atmos. Res.*, 163, 74 – 90, <https://doi.org/https://doi.org/10.1016/j.atmosres.2014.12.014>, <http://www.sciencedirect.com/science/article/pii/S0169809515000034>, 6th Workshop of the International Precipitation Working Group, 2015.

- Klepp, C., Michel, S., Protat, A., Burdanowitz, J., Albern, N., Louf, V., Bakan, S., Dahl, A., and Thiele, T.: Ocean Rainfall And Ice-phase precipitation measurement Network - OceanRAIN-M, <https://doi.org/10.1594/WDCC/OceanRAIN-M>, 2017.
- Klepp, C., Michel, S., Protat, A., Burdanowitz, J., Albern, N., Kähnert, M., Dahl, A., Louf, V., Bakan, S., and Buehler, S. A.: OceanRAIN, a new in-situ shipboard global ocean surface-reference dataset of all water cycle components, *Sci. Data*, 5, 180 122, <https://doi.org/10.1038/sdata.2018.122>, 2018.
- Kummerow, C. D., Randel, D. L., Kulie, M., Wang, N.-Y., Ferraro, R., Joseph Munchak, S., and Petkovic, V.: The evolution of the Goddard profiling algorithm to a fully parametric scheme, *J. Atmos. Oceanic Technol.*, 32, 2265–2280, <https://doi.org/10.1175/JTECH-D-15-0039.1>, 2015.
- Lebsock, M. D., Stephens, G. L., and Kummerow, C.: Multisensor satellite observations of aerosol effects on warm clouds, *J. Geophys. Res. Atmos.*, 113, <https://doi.org/10.1029/2008JD009876>, 2008.
- Leinonen, J., Moisseev, D., Leskinen, M., and Petersen, W. A.: A Climatology of Disdrometer Measurements of Rainfall in Finland over Five Years with Implications for Global Radar Observations, *J. Appl. Meteorol. Climatol.*, 51, 392–404, <https://doi.org/10.1175/JAMC-D-11-056.1>, 2012.
- Loew, A., Bell, W., Brocca, L., Bulgin, C. E., Burdanowitz, J., Calbet, X., Donner, R. V., Ghent, D., Gruber, A., Kaminski, T., Kinzel, J., Klepp, C., Lambert, J.-C., Schaepman-Strub, G., Schröder, M., and Verhoelst, T.: Validation practices for satellite-based Earth observation data across communities, *Rev. Geophys.*, 55, 779–817, <https://doi.org/10.1002/2017RG000562>, <https://agupubs.onlinelibrary.wiley.com/doi/abs/10.1002/2017RG000562>, 2017.
- Marshall, J. S. and Palmer, W. M. K.: The distribution of raindrops with size, *J. Meteor.*, 5, 165–166, [https://doi.org/10.1175/1520-0469\(1948\)005<0165:TDORWS>2.0.CO;2](https://doi.org/10.1175/1520-0469(1948)005<0165:TDORWS>2.0.CO;2), 1948.
- Mason, S. L., Chiu, J. C., Hogan, R. J., and Tian, L.: Improved rain rate and drop size retrievals from airborne Doppler radar, *Atmos. Chem. Phys.*, 17, 11 567—11 589, <https://doi.org/10.5194/acp-17-11567-2017>, 2017.
- Maze, G., Mercier, H., Fablet, R., Tandeo, P., Radcenco, M. L., Lenca, P., Feucher, C., and Goff, C. L.: Coherent heat patterns revealed by unsupervised classification of Argo temperature profiles in the North Atlantic Ocean, *Prog. Oceanogr.*, 151, 275–292, <https://doi.org/https://doi.org/10.1016/j.pocean.2016.12.008>, <http://www.sciencedirect.com/science/article/pii/S0079661116300714>, 2017.
- Munchak, S. J., Kummerow, C. D., and Elsaesser, G.: Relationships between the raindrop size distribution and properties of the environment and clouds inferred from TRMM, *J. Climate*, 25, 2963–2978, <https://doi.org/10.1175/JCLI-D-11-00274.1>, 2012.
- Olson, W.: GPM DPR and GMI (Combined Precipitation) L3 1 month 0.25 degree x 0.25 degree V06, <https://doi.org/10.5067/GPM/DPRGMI/CMB/3B-MONTH/06>, [https://disc.gsfc.nasa.gov/datasets/GPM\\_3CMB\\_06](https://disc.gsfc.nasa.gov/datasets/GPM_3CMB_06), 2017.
- Pedregosa, F., Varoquaux, G., Gramfort, A., Michel, V., Thirion, B., Grisel, O., Blondel, M., Prettenhofer, P., Weiss, R., Dubourg, V., Vanderplas, J., Passos, A., Cournapeau, D., Brucher, M., Perrot, M., and Duchesnay, E.: Scikit-learn: Machine Learning in Python, *J. Mach. Learn. Res.*, 12, 2825–2830, 2011.
- Petersen, W. A., Kirstetter, P. E., Wang, J., Wolff, D. B., and Tokay, A.: The GPM Ground Validation Program, in: *Satellite Precipitation Measurement*, chap. 4.2, Springer Nature, in press.
- Petković, V., Kummerow, C. D., Randel, D. L., Pierce, J. R., and Kodros, J. K.: Improving the Quality of Heavy Precipitation Estimates from Satellite Passive Microwave Rainfall Retrievals, *J. Hydrometeorol.*, 19, 69–85, <https://doi.org/10.1175/JHM-D-17-0069.1>, 2018.
- Petty, G. W. and Huang, W.: The Modified Gamma Size Distribution Applied to Inhomogeneous and Nonspherical Particles: Key Relationships and Conversions, *J. Atmos. Sci.*, 68, 1460–1473, <https://doi.org/10.1175/2011JAS3645.1>, 2011.

- Prigent, C., Aires, F., Wang, D., Fox, S., and Harlow, C.: Sea-surface emissivity parametrization from microwaves to millimetre waves, *Quart. J. Roy. Meteor. Soc.*, 143, 596–605, <https://doi.org/10.1002/qj.2953>, 2017.
- Schwarz, G.: Estimating the Dimension of a Model, *Ann. Stat.*, 6, 461–464, <https://doi.org/10.1214/aos/1176344136>, 1978.
- Smith, P. L.: Raindrop Size Distributions: Exponential or Gamma—Does the Difference Matter?, *J. Appl. Meteorol.*, 42, 1031–1034, [https://doi.org/10.1175/1520-0450\(2003\)042<1031:RSDEOG>2.0.CO;2](https://doi.org/10.1175/1520-0450(2003)042<1031:RSDEOG>2.0.CO;2), 2003.
- Tapiador, F. J., Haddad, Z. S., and Turk, J.: A Probabilistic View on Raindrop Size Distribution Modeling: A Physical Interpretation of Rain Microphysics, *J. Hydrometeorol.*, 15, 427–443, <https://doi.org/10.1175/JHM-D-13-033.1>, 2014.
- Testud, J., Oury, S., Black, R. A., Amayenc, P., and Dou, X.: The concept of “normalized” distribution to describe raindrop spectra: A tool for cloud physics and cloud Remote Sens., *J. Appl. Meteorol.*, 40, 1118–1140, [https://doi.org/10.1175/1520-0450\(2001\)040<1118:TCONDNT>2.0.CO;2](https://doi.org/10.1175/1520-0450(2001)040<1118:TCONDNT>2.0.CO;2), 2001.
- Thompson, E. J., Rutledge, S. A., Dolan, B., and Thurai, M.: Drop Size Distributions and Radar Observations of Convective and Stratiform Rain over the Equatorial Indian and West Pacific Oceans, *J. Atmos. Sci.*, 72, 4091–4125, <https://doi.org/10.1175/JAS-D-14-0206.1>, 2015.
- Thompson, E. J., Rutledge, S. A., Dolan, B., Thurai, M., and Chandrasekar, V.: Dual-Polarization Radar Rainfall Estimation over Tropical Oceans, *J. Appl. Meteorol. Climatol.*, 57, 755–775, <https://doi.org/10.1175/JAMC-D-17-0160.1>, 2018.
- Thurai, M. and Bringi, V. N.: Application of the Generalized Gamma Model to Represent the Full Rain Drop Size Distribution Spectra, *J. Appl. Meteorol. Climatol.*, 57, 1197–1210, <https://doi.org/10.1175/jamc-d-17-0235.1>, 2018.
- Thurai, M., Bringi, V. N., and May, P. T.: CPOL Radar-Derived Drop Size Distribution Statistics of Stratiform and Convective Rain for Two Regimes in Darwin, Australia, *J. Atmos. Oceanic Technol.*, 27, 932–942, <https://doi.org/10.1175/2010JTECHA1349.1>, 2010.
- Thurai, M., Gatlin, P., Bringi, V., Petersen, W., Kennedy, P., Notaroš, B., and Carey, L.: Toward completing the raindrop size spectrum: Case studies involving 2D-video disdrometer, droplet spectrometer, and polarimetric radar measurements, *J. Appl. Meteorol. Climatol.*, 56, 877–896, <https://doi.org/10.1175/JAMC-D-16-0304.1>, 2017.
- Ulbrich, C. W.: Natural variations in the analytical form of the raindrop size distribution, *J. Climate Appl. Meteor.*, 22, 1764–1775, [https://doi.org/10.1175/1520-0450\(1983\)022<1764:NVITAF>2.0.CO;2](https://doi.org/10.1175/1520-0450(1983)022<1764:NVITAF>2.0.CO;2), 1983.
- Williams, C. R.: Reflectivity and Liquid Water Content Vertical Decomposition Diagrams to Diagnose Vertical Evolution of Raindrop Size Distributions, *J. Atmos. Oceanic Technol.*, 33, 579–595, <https://doi.org/10.1175/JTECH-D-15-0208.1>, 2016.
- Williams, C. R. and Gage, K. S.: Raindrop size distribution variability estimated using ensemble statistics, *Ann. Geophys.*, 27, 555–567, <https://doi.org/10.5194/angeo-27-555-2009>, <https://www.ann-geophys.net/27/555/2009/>, 2009.
- Williams, C. R., Bringi, V. N., Carey, L. D., Chandrasekar, V., Gatlin, P. N., Haddad, Z. S., Meneghini, R., Munchak, S. J., Nesbitt, S. W., Petersen, W. A., Tanelli, S., Tokay, A., Wilson, A., and Wolff, D. B.: Describing the Shape of Raindrop Size Distributions Using Uncorrelated Raindrop Mass Spectrum Parameters, *J. Appl. Meteorol. Climatol.*, 53, 1282–1296, <https://doi.org/10.1175/JAMC-D-13-076.1>, 2014.